Cerebellar tDCS differentially modulates sensory inputs in somatosensory cortex and cerebellum.

Carlos Andrés Sánchez-León[1,2], Isabel Cordones[1], Alba Jiménez-Díaz[3], Guy Cheron[4], Javier F Medina[5] and Javier Márquez-Ruiz [1]

[1] Department of Physiology, Anatomy and Cell Biology, Pablo de Olavide University, Ctra. de Utrera, km. 1, 41013, Seville, Spain. [2] Department of Neurology and Neurobiology, University of California Los Angeles, Los Angeles 90095, USA. [3] Department of Personality, Assessment and Psychological Treatments, Faculty of Psychology, University of Valencia, 46010, Valencia, Spain. [4] Université Libre de Bruxelles, Brussels, Belgium. [5] Department of Neuroscience, Baylor College of Medicine, Houston, TX, USA.

Running title: Cb-tDCS effects on sensory inputs

Acknowledgements: This work was supported by grants from the Spanish MINECO-FEDER (BFU2014-53820-P and BFU2017-89615-P) to J.M-R and from the US National Institutes of Health (RF1MH114269) to J.F.M and J.M-R. C.A.S-L was in receipt of an FPU grant from the Spanish Government (FPU13/04858).

Corresponding author:
Javier Márquez-Ruiz, Ph.D.
Brain Stimulation translational Laboratory
Universidad Pablo de Olavide
Ctra. de Utrera, km. 1
41013-Sevilla, Spain
E-mail: jmarquez@upo.es
Phone: +34-954-978054

Declaration of interests: The authors declare no competing financial interests.

Abstract

Cerebellar transcranial direct-current stimulation (Cb-tDCS) is a promising tool for non-invasive modulation of cerebellar activity and has been proposed for the treatment of cerebellum-related disorders. However, how external currents applied to the cerebellum affect local and distant circuits remains unclear. In this study, we examined the immediate and aftereffects of Cb-tDCS on sensory inputs recorded in the cerebellar Crus I/II and primary somatosensory cortex (S1) in response to whisker stimulation. We also assessed changes in the excitation/inhibition balance using vGLUT1 and GAD 65–67 immunoreactivity. Anodal and cathodal Cb-tDCS respectively induced an immediate increase and decrease in the trigeminal component in Crus I/II but no aftereffects were observed 20 minutes post-stimulation. In S1, Cb-tDCS resulted in polarity-dependent modulation of the N1 component during stimulation, which was opposite to the changes induced in Crus I/II and a sustained increase after anodal Cb-tDCS, accompanied by reduced GAD 65–67 immunoreactivity. While power spectrum analysis revealed no changes in Crus I/II, cathodal Cb-tDCS significantly modulated gamma (30–45 Hz) and high-frequency oscillations (255–300 Hz) in S1. These findings indicate that Cb-tDCS can modulate sensory inputs during stimulation and exert delayed effects in distant cortical areas, emphasizing the need to consider both online and remote network modulation in clinical applications.

Introduction

The cerebellum, traditionally associated with motor coordination and learning (Ito, 2002), has increasingly been recognized for its involvement in sensory processing and cognitive functions (Schmahmann & Sherman, 1998; Schmahmann, 2001; Ramnani, 2006; Bostan & Strick, 2018). Transcranial direct-current stimulation (tDCS) is a non-invasive brain stimulation technique that modulates neural excitability through the application of weak direct currents to the scalp (Nitsche & Paulus, 2000; Woods et al., 2016). Recent studies have demonstrated the efficacy of tDCS in modulating cortical excitability and inducing neuroplasticity in various brain regions (Stagg et al., 2018), including the cerebellum (Galea et al., 2009). Cerebellar tDCS (Cb-tDCS) has been shown to modulate motor, cognitive, and emotional behaviors by engaging distinct cerebellar circuits (Grimaldi et al., 2016). As a result, it has been suggested as a promising noninvasive neuromodulatory therapy for disorders involving cerebellar dysfunction (Manto et al., 2022). However, the specific effects of Cb-tDCS on sensory inputs remain poorly understood.

Understanding the neural mechanisms that underlie sensory processing is crucial to unraveling the complexities of perception and cognition. Previous research has implicated the cerebellum in sensory integration and processing of a wide range of sensory modalities, including visual, auditory, and somatosensory inputs (Baumann et al., 2015). However, the precise contribution of cerebellar activity to sensory processing and how it can be modulated by tDCS remains largely unexplored. Previous studies on tDCS have demonstrated its ability to modulate the amplitude of sensory-evoked potentials (SEPs) in both humans (Matsunaga et al., 2004; Dieckhöfer et al., 2006) and animals (Márquez-Ruiz et al., 2012; Sánchez-León et al., 2021). SEPs can be measured in the primary somatosensory cortex (S1) of both humans (Sugawara et al., 2015; Vaseghi et al., 2015) and rodents (Castro-Alamancos & Bezdudnaya, 2015), underscoring their importance as a valuable tool for translational studies (Sánchez-León et al., 2018). In addition to S1, SEPs can also be recorded in CrusI/II region of the cerebellum (Mapelli & D'Angelo, 2007; Roggeri et al., 2008; Márquez-Ruiz & Cheron, 2012; Fernández et al., 2021) with several components that reflect inputs from the trigeminal ganglion and cerebral cortex (Morissette & Bower, 1996; Brown & Bower, 2002). S1 is highly interconnected with the cerebellum (Schmahmann, 2001; Ramnani, 2006; Buckner et al., 2011), with information reaching the cerebellar cortex through its two inputs, from the mossy

fibers through the pontine nucleus (Allen et al., 1979; Leergaard et al., 2000; Nagao, 2004; Odeh et al., 2005) and from the climbing fibers through the inferior olive (Swenson et al., 1989; Lawrenson et al., 2016). Furthermore, the cerebellum projects to S1 through the thalamus (Proville et al., 2014), closing the loop between these two areas.

Cerebellar-brain inhibition refers to a neural pathway through which the cerebellum can exert inhibitory control over other areas of the brain (Ugawa et al., 1991). This pathway involves inhibitory Purkinje cells (PC) in the cerebellar cortex, which receive input from various sensory and motor systems. These PCs send inhibitory signals to deep cerebellar nuclei, including fastigial, interposed, and dentate nuclei (Sugihara, 2011). Subsequently, these nuclei send excitatory signals to the thalamus (Gornati et al., 2018), which then modulates the activity of different regions of the brain, including the cerebral cortex and basal ganglia (Bostan et al., 2013). Unraveling the mechanisms and functions of cerebellar-brain inhibition is essential for advancing our knowledge of brain function and fostering the development of effective therapies for neurological disorders.

In this study, we aim to investigate the local and distant effects of Cb-tDCS on sensory inputs in awake mice. For that, we recorded the SEPs induced by whisker stimulation in Crus I/II and S1 before, during, and after the application of short (15 s) or long (20 min) sessions of Cb-tDCS. To identify molecular changes induced by Cb-tDCS, we performed a post-stimulation immunohistochemical analysis of the immunoreactivity of GAD 65–67 and vGLUT1 in the stimulated brain region. Our findings provide valuable insights into the role of the cerebellum in sensory processing and have broad implications for the development of novel therapeutic strategies targeting sensory disorders.

Material and Methods

Animals. Experiments were conducted on adult male C57 mice (University of Seville, Spain) weighing 28–35 g. All experimental procedures were carried out in accordance with European Union guidelines (2010/63/CE) and followed the Spanish regulations (RD 53/2013 and RD 118/2021) regarding the use of laboratory animals in chronic experiments. Furthermore, these experiments were submitted to and approved by the local Ethics Committee of Pablo de Olavide University (Seville, Spain).

Surgery. Mice were prepared for the chronic recording of SEPs in Crus I/II and S1, along with simultaneous Cb-tDCS, following established protocols (Sun et al., 2020; Sánchez-León et al., 2021, 2023). The mice were initially anesthetized with a ketamine–xylazine mixture (Ketaset, 100 mg/ml, Zoetis, NJ., USA; Rompun, 20 mg/ml, Bayer, Leverkusen, Germany) at an initial dosage of 0.1 ml/20 g. Under aseptic conditions, a midline anteroposterior (AP) incision was made along the head, from the front leading edge to the lambdoid suture. The periosteum of the exposed skull surface was then removed and rinsed with saline. The animal's head was positioned accurately to mark the bregma as the stereotaxic zero reference point. In the experiments where SEPs were recorded in Crus I/II during simultaneous Cb-tDCS, a custom-made silver ring chlorinated electrode (2.5 mm inner diameter, 3.5 mm outer diameter) was placed over the left Crus I/II region on the skull (AP = − 6 mm; Lateral = +2 mm; relative to bregma (Paxinos & Franklin, 2013)) (Fig. 1A). The electrode served as the active electrode for Cb-tDCS and was secured with dental cement (DuraLay, Ill., USA), without filling the gap between the electrode and the skull. Additionally, a hole (2 mm diameter) was drilled in the interparietal bone within the ring electrode to expose the cerebellum, and the dura mater surface was protected with wax bone (Ethicon, Johnson & Johnson, NJ., USA). In experiments where SEPs were recorded in S1 during simultaneous Cb-tDCS, the active electrode for tDCS was a polyethylene tubing (inner diameter: 2.159 mm; outer diameter: 3.251 mm; A-M Systems) placed over the stimulated region (AP = − 6 mm; Lateral = +2 mm; relative to bregma (Paxinos & Franklin, 2013)) and filled with electrogel in which the electrode from the stimulator was immersed (Fig. 5A). A hole (2 mm diameter) was drilled in the right parietal bone, centered on the right S1 vibrissa area (AP = − 0.9 mm; Lateral = − 3 mm; relative to bregma (Paxinos & Franklin, 2013)), and the dura mater surface was protected with wax bone. Furthermore, a silver electrode was implanted over the dura surface beneath the left parietal bone (AP = − 0.9 mm; Lateral = + 3 mm; relative to bregma (Paxinos & Franklin, 2013)) to serve as the electrical reference for the electrophysiological recordings. The electrode was constructed by cutting a silver wire (381 µm diameter, A-M Systems) into 1 cm pieces. A 2 mm diameter loop was formed at one end to facilitate grasping by the amplifier system, while the opposite end was braided and filed to prevent damage to the dura mater. For the histological experiments, the active electrode for Cb-tDCS consisted of a polyethylene tubing as described earlier. No trepanation was performed in the histological experiments to prevent

tissue damage. Finally, a head-holding system, comprising three bolts screwed into the skull and an upside-down bolt placed over the skull perpendicular to the horizontal plane, was implanted to allow for head fixation during the experiments. The complete holding system was cemented to the skull to ensure stable head positioning.

Recording and stimulation procedures. Recording sessions commenced at least two days after the surgical procedure. The mice were placed on a treadmill equipped with an infrared sensor to monitor locomotion activity. The head was securely fixed to the recording table using the implanted head-holding system. To stimulate the whiskers, an electrical stimulus (0.2 ms square pulse, < 2.5 mA) was delivered through a pair of hook electrodes inserted in the left whisker pad. The electrodes were connected to an isolation unit (CS20, Cibertec, Madrid, Spain) controlled by a stimulator device (CS420, Cibertec). For characterizing the SEPs, a glass micropipette (1-5 MΩ of impedance; outer diameter: 2.0 mm; inner diameter: 1.6 mm; length: 15 cm, with inner filament; A-M Systems, WA., USA) filled with 3M NaCl was mounted on a micromanipulator (MO-10, Narishige, Tokyo, Japan) and positioned over S1 area. The electrical stimulus was delivered to the whisker pad every 10 ± 2 s while the micropipette was gradually lowered and the current intensity adjusted (0.7 - 2.5 mA) until the maximum amplitude SEP was achieved. Subsequently, the current intensity of the whisker electrical pulses was reduced to elicit a SEP with half of the maximum amplitude. This allowed for the observation of changes in the components of the SEP during and after Cb-tDCS intervention. All recordings were acquired using an amplifier (BVC-700A, Dagan corporation, MN., USA) connected to a dual extracellular-intracellular headstage (8024, Dagan corporation; gain error ± 1 %, noise 4.5 µV root mean square). The sampling rate was set at 25 kHz, and the amplitude resolution was 12 bits (CED Micro 1401; Cambridge Electronic Design, Cambridge, UK).

Transcranial electrical stimulation. The different protocols for transcranial currents were designed in Spike2 software (Cambridge Electronic Design (CED), Cambridge, U.K.) and transmitted to a battery-powered linear stimulus isolator (WPI A395, Fl., USA). Cb-tDCS was applied between the ring electrode (in the experiments combining SEP recording in Crus I/II) or the plastic tubing (in experiments combining SEP recording in S1) placed over Crus I/II. A reference electrode consisting of a rubber rectangle (6 cm^2) moistened with electrogel

(Electro-Cap International, OH., USA) was attached to the back of the mouse. A silver wire was inserted into the rubber electrode for connection to the stimulator. To assess the immediate effects induced by Cb-tDCS, 15 s pulses of anodal and cathodal tDCS were applied with a 10-second gap of non-stimulation between them. Cb-tDCS was delivered at 200 µA to assess local effects in the cerebellum and at 200 and 300 µA to evaluate changes in S1. For assessing after-effects changes in Crus I/II, Cb-tDCS was delivered for 20 min at 200 µA for cathodal stimulation, 20 min at 200 µA for anodal stimulation, and for 30 s at 200 µA anodal for sham stimulation. To evaluate after-effects changes in S1, Cb-tDCS was administered for 20 min at 300 µA for cathodal stimulation, 20 min at 300 µA for anodal stimulation, and for 30 s at 300 µA anodal for sham stimulation. The current was directly monitored during experiments to ensure that it matched the desired level indicated in the stimulator.

Histology. To examine potential histological changes in Crus I/II and S1 associated with Cb-tDCS, a separate group of animals received 20 min of anodal, cathodal, or sham Cb-tDCS at 300 µA. Fifteen min after cessation of Cb-tDCS, mice were deeply anesthetized with a ketamine–xylazine mixture (Ketaset, 100 mg/ml; Rompun, 20 mg/ml) and transcardially perfused with 0.9% saline, followed by 4% paraformaldehyde (PanReac, Barcelona, Spain) in PBS. The brains were then extracted and stored in 4% paraformaldehyde for 24 hours. Subsequently, they were cryoprotected in 30% sucrose in PB for the next 48 hours and then sectioned into 50 µm coronal slices using a freezing microtome (CM1520, Leica, Wetzlar, Germany). After three 10-min washes with PBS, sections were blocked with 10% Normal Donkey Serum (NDS, 566460, Merck, Darmstadt, Germany) in PBS containing 0.2% Triton X-100 (Sigma-Aldrich, Mo., USA) (PBS-Tx-10% NDS). They were then incubated overnight at room temperature in darkness with mouse anti-vesicular Glutamate Transporter 1 (vGLUT1, 1:1000, MAB5502, Merck) or rabbit anti-Glutamate Decarboxylase 65-67 (GAD 65-67, 1:1000, AB1511, Merck). After three washes, the sections were incubated for 1 hour at room temperature in darkness with appropriate secondary antibodies: Alexa Fluor 488 donkey anti-mouse IgG (H+L) (1:400, A21202, Thermo Fisher Scientific, Mass., USA) or Alexa Fluor 555 donkey anti-rabbit IgG (H+L) (1:400, A31572, Thermo Fisher Scientific) in PBS-Tx-5% NDS. Following three washes with PBS, the sections were mounted on glass slides and coverslipped, and confocal images were acquired using a confocal microscope (A1R HD25, Nikon, Tokyo, Japan).

Data analysis. SEP amplitude was computed using the peak-to-peak command in Spike2 software, where the maximum negative voltage value (N1) was subtracted from the maximum positive voltage value (P1) of the preceding peak. SEPs recorded when the animal was running were excluded from the analysis, as well as potentials containing electrical artifacts.

Confocal images were processed using Fiji software (http://fiji.sc/Fiji) with a custom-built macro. The fluorescence background was subtracted, and five square regions of interest (ROI) measuring 100 x 100 pixels (291.31 μm^2) were randomly placed in areas without nuclei or nonspecific noise, such as blood vessels. Each image within the ROI was converted to binary, and the "Analyze Particles" command was utilized to count and measure aggregates of vGLUT1 and GAD 65-67. The particle count was averaged to obtain one value per hemisphere per animal.

To analyze the spectral dynamics of the neural oscillations using the Fast Fourier Transform (FFT) an analysis of the *induced activity* was performed. The average SEP from each subject was subtracted from each condition, temporal period, and subject (Bastiaansen & Hagoort, 2003; Tallon-Baudry & Bertrand, 1999). Power spectrum computation was carried out using the FieldTrip toolbox (Oostenveld et al., 2011), employing the fast Fourier transform (multitaper method) for frequencies ranging from 3 to 300 Hz. Power spectrum values were extracted from each trial and averaged for each animal and temporal period. The calculated power was referenced to power obtained during the control period, resulting in the ratio of the power spectrum during each temporal period relative to the control period for each subject. Spectral power was then determined for specific power bands: theta (4-10 Hz), beta (10-30 Hz), low gamma (30-45 Hz), high gamma (60-100 Hz), HFO1 (100-145 Hz), HFO2 (155-200 Hz), HFO3 (200-245 Hz) and HFO4 (255-300 Hz). These ratios were averaged within each group. Power bands from 20 min post-tDCS (Post1) and 40 min post-tDCS (Post2) were compared to the control period.

Statistical analysis was conducted using SigmaPlot 11.0 (Systat Software Inc, San Jose, CA., USA), IBM SPSS version 25 (IBM, Armonk, NY)) and Matlab 2015a (MathWorks Inc.). Normality was assessed using the Shapiro–Wilk test (P value > 0.05). For immediate effect experiments, one-sample t-tests were employed to assess the statistical significance of tDCS effects, with normalized values during tDCS compared against a theoretical mean of 100 for

amplitude and 0 for latency, followed by a 2-way Repeated Measures ANOVA to determine the statistical significance of differences between groups, with POLARITY (anodal vs cathodal) and COMPONENT (T vs C) as within subject factors for cerebellar SEP analysis, and POLARITY (anodal vs cathodal) and INTENSITY (200 µA VS 300 µA) for S1 SEP analysis, with post hoc uncorrected Fisher's LSD test for multiple comparisons. For after-effects experiments, Repeated Measures ANOVA or Friedman Repeated Measures Analysis of Variance on Ranks, followed by Dunnett's post hoc test when data did not fit a normal distribution, were employed to infer the statistical significance of differences. Immunohistochemical experiments utilized a two-way mixed ANOVA with BRAIN HEMISPHERE (non-stimulated vs. stimulated hemisphere) as a within-subject factor and tDCS POLARITY (anodal, cathodal, or sham) as a between-subjects factor to compare fluorescence levels. For power spectrum analysis, a one-sample t-test was used to determine significant differences. The results are presented as mean ± SEM, and statistical significance was set at $p < 0.05$ for all analyses.

Results

Characterization of cerebellar SEPs in response to whisker stimulation.

To assess potential changes in neuronal excitability within the Crus I/II region of the cerebellum during and after tDCS, SEPs in response to whisker stimulation were chronically recorded in awake, head-restrained mice (N = 14; Fig. 1A). Electrical stimulation of the whisker evoked an ipsilateral short-latency SEP in the Crus I/II, characterized by two prominent negative waves corresponding to trigeminal (T) and cortical (C) responses, peaking at 3.79 ± 0.69 ms and 12.57 ± 1.12 ms, respectively (Fig. 1B). The amplitudes of these SEP components demonstrated a linear relationship with the intensity of the electrical stimuli applied to the whiskers, as depicted in Figure 1C. The correlation coefficients for the T and C components were $R = 0.98$ ($p < 0.0001$, N = 2) and $R = 0.93$ ($p = 0.0002$, N = 2), respectively (Fig. 1D,E). During the experiments, the final current intensity applied to the whiskers was adjusted to elicit a T component with half of the maximum amplitude, allowing for modulation of the SEP amplitude during and after Cb-tDCS intervention.

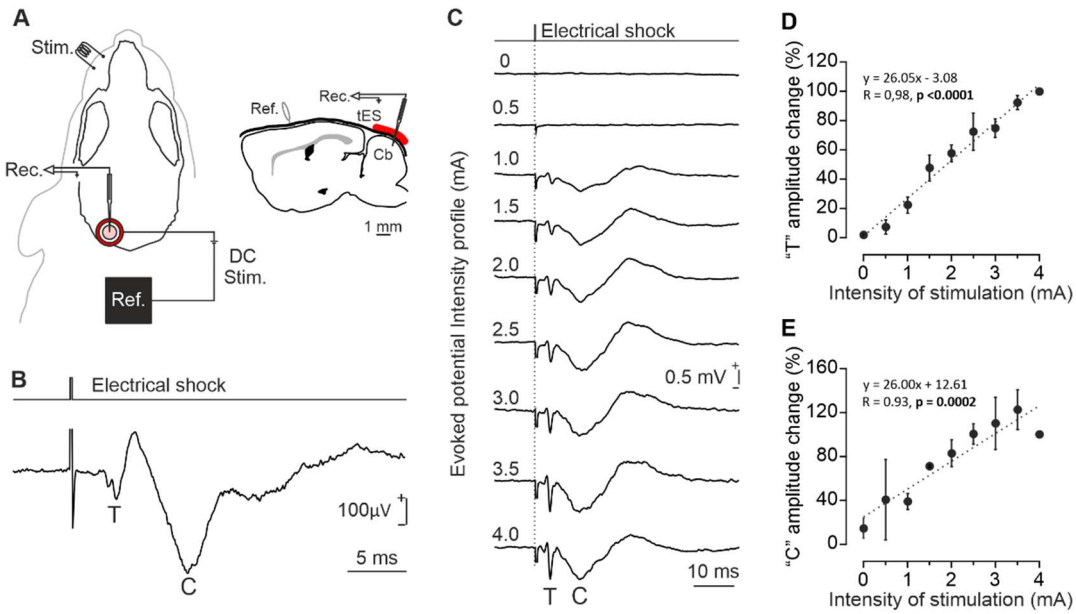

Figure 1. Sensory evoked potential (SEP) characterization in Crus I/II. *A*) Experimental setup for concurrent Cb-tDCS and *in vivo* electrophysiological recordings in Crus I/II. The right side shows a schematic representation of the active electrode and recording site in the lateral cerebellum. *B*) Representative profile of Crus I/II SEP induced by whisker electrical stimulation. The graph displays the different trigeminal (T) and cortical (C) components (n = 30 SEPs from a representative mouse). *C*) Intensity profile of Crus I/II-SEP. Each trace represents an average of 5 SEPs recorded at the same location but with varying intensities of whisker electrical stimulation. *D*) Quantification of amplitude changes in the T component of SEPs at different intensities of whisker electrical stimulation. Data normalized to the maximum amplitude recorded at 4 mA (N = 2 mice). E) Quantification of amplitude changes in the C component of SEPs at different intensities of whisker electrical stimulation. Data normalized to the maximum amplitude recorded at 4 mA (N = 2 mice). Cb: cerebellum; Rec.: recording; Ref.: reference; Stim.: stimulation; tES: transcranial electrical stimulation.

Cb-tDCS modulates the amplitude of SEPs recorded in the cerebellum during its application but does not cause observable long-term effects.

To test the immediate effects of Cb-tDCS on Crus I/II excitability we recorded SEPs induced by whisker pad stimulation during simultaneous short-duration (15 s, including 5 s ramp up and 5 s ramp down) anodal and cathodal tDCS pulses (± 200 µA) (Fig. 2A). The calculated density current for the used tDCS intensity was 4.26 mA/cm^2. The peak-to-peak amplitudes and the latencies of the T and C components of SEPs recorded just before Cb-tDCS pulses were compared with those recorded during Cb-tDCS application. Figure 2A shows the averaged SEPs (n = 30) during anodal (dark red trace) and cathodal (dark blue trace) Cb-tDCS, as well as the control conditions for anodal (light red trace) and cathodal (light blue trace), for a representative animal. Mean data obtained from the group of animals participating in the

experiment (N = 10) for T and C components are represented in Figure 2B,C. Data was normalized by the values during the control condition for anodal or cathodal stimulation. For the amplitude values of the T component, anodal and cathodal polarities modulated SEP amplitudes in opposite directions, showing a significant increase during anodal stimulation (one-sample t-test, t_9 = 3.094, p = 0.013) and a significant decrease during cathodal stimulation (one-sample t-test, t_9 = 3.506, p = 0.007). Thus, anodal Cb-tDCS increased on average to 111.2 ± 3.61 % the amplitude of simultaneously recorded T component, whereas cathodal Cb-tDCS significantly decreased T component amplitude to 86.13 ± 3.96 % at 200 µA (Fig. 2B). Although the cortical component shows a tendency to be modulated by Cb-tDCS in the opposed direction than the trigeminal one (anodal Cb-tDCS decreased its amplitude to 88.57 ± 7.38 %, whereas cathodal Cb-tDCS increased it to 103.2 ± 6.205 %), these differences were not statistically significant (p = 0.156 for anodal; p = 0.618 for cathodal; Fig. 2B). Next, we compared the amplitude values between the T and C components, and between anodal and cathodal stimulation. The 2-way RM ANOVA revealed a main effect for the interaction POLARITY x COMPONENT, but not the factors POLARITY or COMPONENT alone (2-way RM ANOVA, POLARITY: $F_{1,9}$ = 0.619, p = 0.452; COMPONENT: $F_{1,9}$ = 0.262, p = 0.621; POLARITY x COMPONENT: $F_{1,9}$ = 22.19, p = 0.001). Post-hoc test (uncorrected Fisher's LSD test; Fig. 2B) revealed significant differences between T and C components for both, Anodal (p = 0.006) and Cathodal (p = 0.046) stimulation, as well as between anodal and cathodal for the T component (p = 0.001), but not for C (p = 0.167). These results show an opposite modulation of the two different cerebellar components, with anodal increasing the T component amplitude and decreasing C, and vice versa for cathodal stimulation, as well as an opposite modulation of the T component for anodal vs cathodal stimulation. For latency comparisons, statistical differences were only found for the T component during anodal Cb-tDCS (one-sample t-test, t_9 = 2.483, p = 0.035; Fig. 2C) showing a negligible increase in latency of 0.06 ms. No statistical changes were observed in the rest of the latency comparisons (one-sample t-test, t_9 = 0.276, p = 0.789 for T component during cathodal; t_9 = 1.010, p = 0.339 for C component during anodal; t_9 = 0.377, p = 0.715 for C component during cathodal). No statistical changes were observed between the latency of T and C components or anodal and cathodal Cb-tDCS (2-way RM ANOVA for T component, POLARITY: $F_{1,9}$ = 1.427, p = 0.263; COMPONENT: $F_{1,9}$ = 0.366, p = 0.560; POLARITY x COMPONENT: $F_{1,9}$ = 1.429, p = 0.263). In summary, the direction of Cb-tDCS effects observed in the amplitude of the trigeminal

component of simultaneously recorded SEPs were dependent on the applied polarity, and an opposite modulation was observed between T and C components.

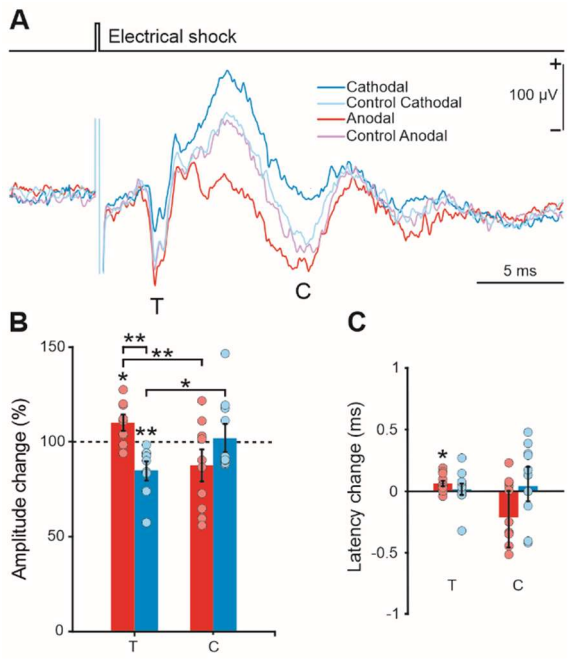

Figure 2. Immediate effects of Cb-tDCS over SEPs in Crus I/II region. *A*) Average SEP (n = 15) recorded in Crus I/II from a representative animal during control before anodal stimulation (light-red trace), anodal (red trace), control before cathodal (light-blue trace), and cathodal (blue trace) Cb-tDCS applied at 4.26 mA/cm2. *B*) Quantification and statistical analysis of Cb-tDCS effects on the amplitude of the trigeminal (T) and cortical (C) components of Crus I/II SEP. The mean (bars) and individual amplitude data (circles) are represented as percentage of change compared to control values for all animals (N = 10 mice). The statistical analysis was performed using one sample t-test and 2-way Repeated Measures ANOVA, with *p < 0.05, **p < 0.01. *C*) Quantification and statistical analysis of the effects of Cb-tDCS on the latency of SEP-components. The mean difference from control values for all animals is represented. Error bars indicate the standard error of the mean (SEM).

To test the potential after-effects of Cb-tDCS over Crus I/II excitability we recorded SEPs induced by whisker pad stimulation (every 10 ± 2 s) in three different randomly assigned experimental conditions, anodal (N = 12), cathodal (N = 11) or sham (N = 7) group. During experimental sessions, SEPs were recorded for 20 min before Cb-tDCS, during continuous anodal (200 µA, 20 min), cathodal (-200 µA, 20 min) or sham (200 µA, 30 s) Cb-tDCS, and for 1 hour after Cb-tDCS. Every 5-minute interval SEP waveforms were averaged and normalized with respect to baseline values (control condition, before Cb-tDCS). As illustrated in Figure 3, Cb-tDCS exerts a significant effect on the normalized T amplitude of SEPs for both anodal (Friedman RM Analysis of Variance on Ranks, $\chi^2_{19} = 53.810$, $p < 0.001$) and cathodal (Friedman

RM Analysis of Variance on Ranks, $\chi^2_{19} = 56.777$, $p < 0.001$) polarities but not Sham stimulation (RM ANOVA, $F_{19,114} = 0.563$, $p = 0.925$). Subsequently, we conducted a comparison of the normalized amplitude change at each time point with respect to the last time point in the baseline condition. Post hoc analysis showed significant differences during the last 10 minutes of Cb-tDCS application for the anodal ($p < 0.05$, Dunnett's post hoc test; N = 12) and cathodal ($p < 0.05$, Dunnett's post hoc test; N = 11) groups. Thus, anodal Cb-tDCS significantly increased the amplitude of the trigeminal component (up to a maximum of 138.58 ± 9.86 %, N = 12) with respect to control values (red-filled diamonds in Fig. 3), whereas cathodal tDCS decreased the amplitude of the trigeminal component with respect to control values reaching its maximum effects (maximum of 85.34 ± 3.68 %, N = 11) during simultaneous tDCS application (blue filled squares in Fig. 3). No differences were found in the amplitude of trigeminal components once Cb-tDCS was switched off. Regarding the analysis of cortical component, no statistical differences were found in any temporal period for anodal (Friedman RM Analysis of Variance on Ranks, $\chi^2_{19} = 16.259$, $p = 0.64$), cathodal (Friedman RM Analysis of Variance on Ranks, $\chi^2_{19} = 8.519$, $p = 0.981$) or Sham (RM ANOVA, $F_{19,76} = 0.815$, $p = 0.683$) Cb-tDCS. In addition, we compared anodal and cathodal amplitude values with those obtained in the sham group. The trigeminal component showed significant differences only between anodal and sham groups restricted to Cb-tDCS application period (One-way ANOVA or Kruskal-Wallis, $p < 0.05$), with no differences in the cathodal CB-tDCS group (asterisk in Fig. 3B). No significant differences were found in the cortical component when comparing anodal or cathodal with the sham group (One-way ANOVA or Kruskal-Wallis). Latency analysis for T and C components showed no significant differences for any of the experimental conditions. Although the Friedman RM Analysis of Variance on Ranks for the latency of T component with anodal stimulation was statistically significant ($\chi^2_{19} = 32.422$, $p = 0.028$), post-hoc tests revealed no significant differences. For cathodal stimulation, the Friedman RM Analysis of Variance on Ranks showed no significant differences for the latency of T component ($\chi^2_{19} = 22.822$, $p = 0.245$). Similarly, no significant differences were found for the latency C component in either anodal ($\chi^2_{19} = 25.416$, $p = 0.147$) or cathodal ($\chi^2_{19} = 23.806$, $p = 0.204$) conditions.

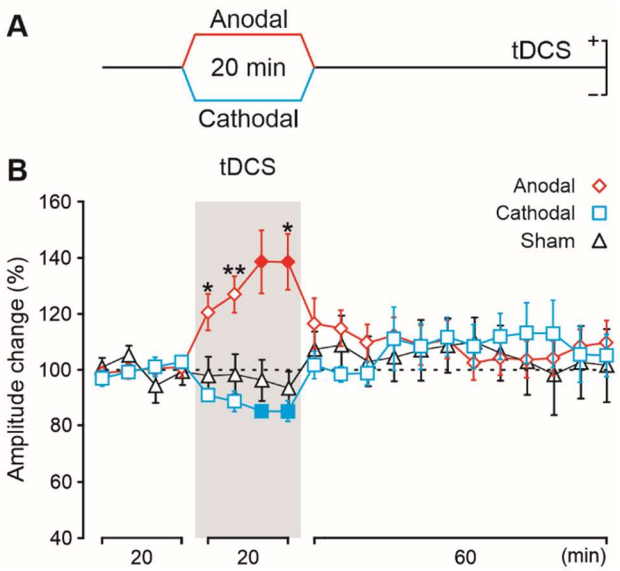

Figure 3. Cb-tDCS after-effects over SEPs in Crus I/II region. *A*) Illustration of the Cb-tDCS protocol applied for long-term experiments (20 min, 4.26 mA/cm^2). *B*) Normalized amplitude change of the trigeminal (T) component, averaged every 5 min for 20 min of anodal (red diamonds), cathodal (blue squares), or sham (black triangles) tDCS. Filled symbols indicate statistical differences compared to the last control period (N = 12 mice for anodal, N = 11 for cathodal, N = 7 mice for sham, $p < 0.05$, Holm-Sidak post hoc test). Asterisks indicate statistical differences between the same temporal period for anodal or cathodal Cb-tDCS compared to sham (N = 12 mice for anodal, N = 11 for cathodal, N = 7 mice for sham, *$p < 0.05$; **$p < 0.01$; ***$p < 0.001$, unpaired t-test). Error bars indicate the standard error of the mean (SEM).

Finally, to explore potential molecular changes induced by Cb-tDCS, we used antibodies against vGLUT1 and GAD 65-67 to assess possible modifications of the excitation/inhibition balance in the transcranially stimulated Crus I/II region. A group of animals prepared for Cb-tDCS application during whisker stimulation (no electrophysiological recordings were carried out in this experiment) was randomly assigned to anodal (N = 7), cathodal (N = 7) or sham (N = 7) conditions. Representative confocal images from the non-stimulated right hemisphere and the transcranially stimulated left hemisphere are presented in Figure 4 for sham (at top), anodal (at middle), and cathodal (at bottom) groups for GAD 65-67 (Fig. 4A) and vGLUT1 (Fig. 4B). The number of GAD 65-67 and vGLUT1 positive clusters of puncta in the stimulated and non-stimulated Crus I/II region were analyzed in the cathodal, anodal and sham groups. Brain hemisphere (non-stimulated vs stimulated hemisphere) and tDCS polarity (anodal, cathodal, or sham) conditions were included in a two-way mixed ANOVA.

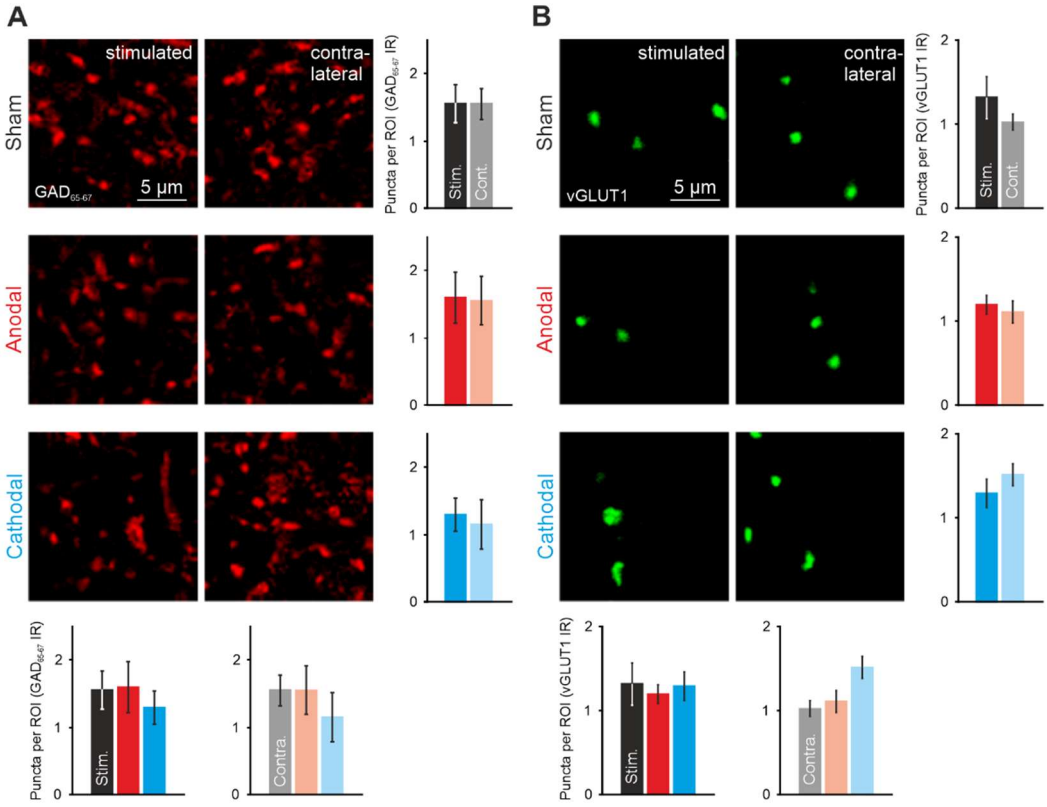

Figure 4. Immunohistochemical immunoreactivity in Crus I/II after 20 minutes of Cb-tDCS. *A,B*) Confocal photomicrographs, quantification, and statistical analysis of GAD 65-67 (*A*) or vGLUT1 immunoreactivity (*B*) in Crus I/II after 20 min of sham condition (upper row, N = 7 mice), anodal Cb-tDCS (middle row, N = 7 mice) and cathodal Cb-tDCS (lower row, N = 7 mice). A comparison of the quantification for the same hemisphere is presented at the bottom. Error bars represent the standard error of the mean (SEM). GAD65-67: Glutamic acid decarboxylase isoforms 65 and 67; vGLUT1: vesicular glutamate transporter 1; ROI: region of interest.

No significant difference in GAD 65-67 nor vGLUT1 was observed after one Cb-tDCS session between the stimulated and non-stimulated hemisphere in any of the tested stimulation conditions (2-way mixed ANOVA for vGLUT1, HEMISPHERE: $F_{1,18}$ =0.223, p = 0.642; POLARITY: $F_{2,18}$ =1.549, p = 0.239; POLARITY x HEMISPHERE: $F_{2,18}$ =1.816, p = 0.191; 2-way mixed ANOVA for GAD 65-67, HEMISPHERE: $F_{1,18}$ =0.075, p = 0.787; POLARITY: $F_{2,18}$ =0.619, p = 0.549; POLARITY x HEMISPHERE: $F_{2,18}$ =0.027, p = 0.973; Fig. 4A, B). This result is consistent with the absence of long-term effects described in the previously mentioned electrophysiological experiments.

Cb-tDCS induces immediate and after-effects on SEPs recorded in S1.

To assess the potential impact of Cb-tDCS on cerebellar-brain inhibition processes, we recorded the SEPs in S1 elicited by whisker pad stimulation (Fig. 5A). Recordings were conducted during simultaneous short-duration (15 s) and throughout the 20-minute period of both anodal and cathodal Cb-tDCS pulses, as well as during the post-stimulation period. Electrical whisker stimulation evoked a contralateral short-latency SEP in the vibrissa S1 area (Fig. 5B) consisting of a first positive component (P1) peaking at 3.18 ± 0.10 ms (N = 8), followed by a negative wave (N1) at 11.73 ± 1.72 ms (N = 8).

To test the immediate effects of Cb-tDCS on S1 excitability we recorded SEPs induced by whisker pad stimulation during simultaneous short-duration (15 s, including 5 s ramp up and 5 s ramp down) anodal and cathodal Cb-tDCS pulses at two different intensities (± 200 and ± 300 µA, equivalent to 5.46 and 8.19 mA/cm^2, respectively). SEPs recorded in S1 just before Cb-tDCS pulses were used as controls to normalize the peak-to-peak amplitude of N1 component in both anodal and cathodal conditions. Figure 5B shows the averaged SEPs (n = 30) during anodal (dark red trace), cathodal (dark blue trace) Cb-tDCS, and the control conditions for anodal (light red trace) and cathodal (light blue trace) at ± 200 and ± 300 µA from a representative animal. Mean data obtained from the groups of animals participating in the experiment (200 µA, N = 11; 300 µA, N = 9) are represented in figure 5C,D (data was normalized by the values during control condition for anodal or cathodal stimulation). We compared the amplitude and latency values during Cb-tDCS stimulation. For 200 µA there was a statistically significant decrease in amplitude values during anodal (one-sample t-test, t_{10} = 2.230, p = 0.049; Fig. 5C) but no differences during cathodal (one-sample t-test, t_{10} = 1.974, p = 0.077; Fig. 5C). Furthermore, at 300 µA stronger effects were observed. Consistent with the observation that anodal and cathodal polarities tend to modulate SEP in opposite directions, we observed a significant decrease in SEP amplitudes during anodal Cb-tDCS (one-sample t-test, t_8 = 3.287, p = 0.011; Fig. 5C) and a significant increase during cathodal Cb-tDCS (one-sample t-test, t_8 = 2.804, p = 0.023; Fig. 5C). Thus, contrary to the observed in the SEPs recorded in Crus I/II region, anodal Cb-tDCS decreased the amplitude of simultaneously recorded N1 component (92.51 ± 3.36 % and 82.69 ± 5.27 % for + 200 µA and + 300 µA, respectively), whereas cathodal Cb-tDCS increased the amplitude (107.41 ± 3.75 % and 118.3 ± 6.61 % for - 200 µA and - 300 µA, respectively). Next, we compared the amplitude values between 200 and 300 µA, and between anodal and cathodal stimulation. The 2-way RM

ANOVA revealed a main effect for the factor POLARITY but not for INTENSITY. Consistent with the observation that anodal and cathodal polarities tend to modulate SEP amplitudes in opposite directions, the interaction POLARITY x INTENSITY was also significant (2-way RM ANOVA, POLARITY: $F_{1,36} = 28.92$, $p < 0.0001$; INTENSITY: $F_{1,36} = 0.019$, $p = 0.892$; POLARITY x INTENSITY: $F_{1,36} = 4.925$, $p = 0.033$). Post-hoc test (uncorrected Fisher's LSD test; Fig. 5C) revealed significant differences between anodal and cathodal stimulation for both, 200 ($p = 0.024$) and 300 µA ($p < 0.0001$) stimulation, but not between the different intensities (Anodal 200 vs 300 µA, $p = 0.150$; Cathodal 200 vs 300 µA, $p = 0.104$). No statistical changes were observed in the latency of N1 component for 200 µA (one-sample t-test, $t_{10} = 0.157$, $p = 0.878$ during anodal; $t_{10} = 0.652$, $p = 0.529$ during cathodal; Fig. 5D), but a significant effect only for anodal at 300 µA (one-sample t-test, $t_8 = 2.495$, $p = 0.037$ during anodal; $t_8 = 0.660$, $p = 0.528$ during cathodal; Fig. 5D) showing a decrease in latency of -0.55 ms ± 0.22 ms. No statistical changes were observed for latencies between anodal and cathodal stimulation or 200 and 300 µA (2-way RM ANOVA, POLARITY: $F_{1,36} = 0.634$, $p = 0.431$; INTENSITY: $F_{1,36} = 0.038$, $p = 0.846$; POLARITY x INTENSITY: $F_{1,36} = 2.556$, $p = 0.119$). In summary, the direction of Cb-tDCS effects observed in the amplitude of the N1 component of simultaneously recorded SEPs in S1 were opposed to those observed in Crus I/II region, and stronger intensity elicited stronger effects. Since short-term effects observed for 200 µA stimulation were weaker and less reliable than during 300 µA, we decided to apply 300 µA for the subsequent experiments.

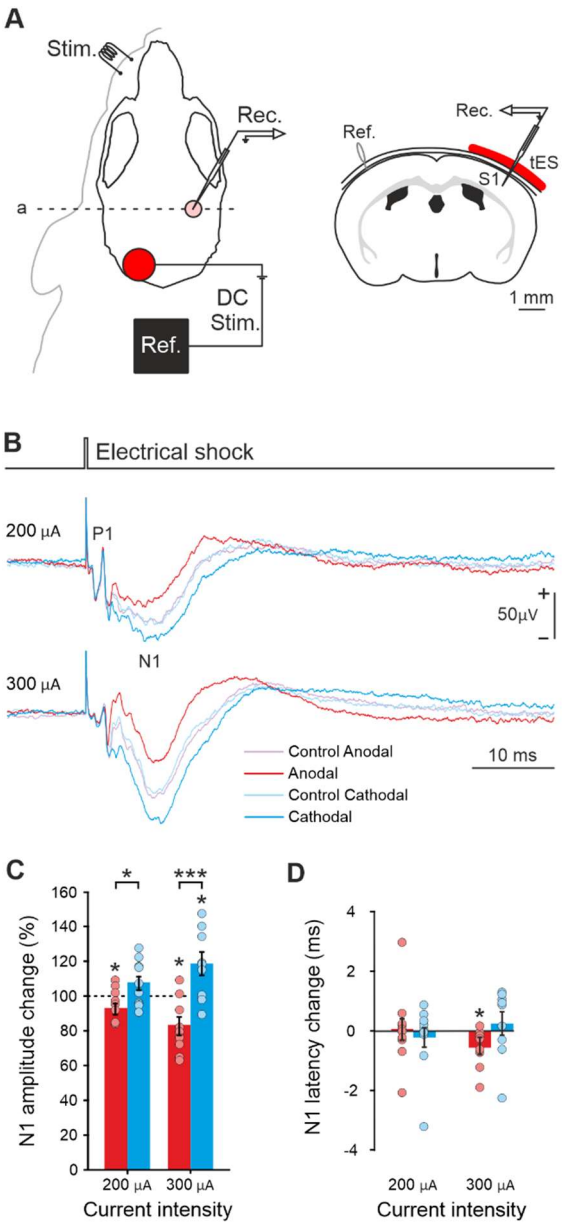

Figure 5. Immediate effects of Cb-tDCS over SEPs in S1. *A*) Experimental setup for concurrent Cb-tDCS and *in vivo* electrophysiological recordings in S1. A schematic coronal representation of the active electrode and recording site in the somatosensory cortex is shown on the right. *B*) Average SEP (n = 15) recorded in S1 from a representative animal during control before anodal stimulation (light-red trace), anodal (red trace), control before cathodal (light-blue trace), and cathodal (blue trace) Cb-tDCS applied at 2.84 mA/cm^2 (upper trace) and 4.26 mA/cm^2 (lower trace). *C*) Quantification and statistical analysis of Cb-tDCS effects on the amplitude of the N1 component of S1 SEP. The mean (bars) and individual amplitude data (circles) are represented as percentage of change compared to control values for all animals (N = 11 mice for 2.84 mA/cm^2, N = 9 for 4.26 mA/cm^2). The statistical analysis was performed using one sample t-test and 2-way Repeated Measures ANOVA, with *$p < 0.05$, ***$p < 0.001$. *D*) Quantification and statistical analysis of the effects of Cb-tDCS on the latency of N1 component of S1 SEP. The mean difference from control values for all animals is represented. Error bars indicate the standard error of the mean (SEM).

To test the potential after-effects of Cb-tDCS on S1 excitability, we recorded SEPs induced by whisker pad stimulation (every 10 ± 2 s) in three different randomly assigned experimental conditions, anodal (N = 5), cathodal (N = 5) or sham (N = 8) group. During experimental sessions, SEPs were recorded in S1 for 20 min before Cb-tDCS, during continuous anodal (+ 300 µA, 20 min), cathodal (- 300 µA, 20 min) or sham (300 µA, 30 s) Cb-tDCS, and for 1 hour after Cb-tDCS. Every 5-minute interval SEP waveforms were averaged and normalized with respect to baseline values (control condition, before Cb-tDCS). As observed in figure 6, Cb-tDCS had a significant effect on the normalized N1 amplitude of SEPs for both anodal (One-way RM ANOVA, $F_{19,76} = 8.840$, $p < 0.001$) and cathodal (Friedman RM Analysis of Variance on Ranks, $\chi^2_{19} = 35.789$, $p = 0.011$) polarity, but not for Sham stimulation (Friedman RM Analysis of Variance on Ranks, $\chi^2_{19} = 26.421$, $p = 0.119$). Subsequently, we conducted a comparison of the normalized amplitude change at each time point with respect to the last time point in the baseline condition. The post hoc analysis showed a significant increase in amplitude after anodal Cb-tDCS application when compared with control values before stimulation ($p < 0.05$, Dunnet post hoc test; red filled diamonds in Fig. 6B) but no differences for multiple comparisons within the cathodal group were found (Dunnet post hoc test; blue squares in Fig. 6B). In addition, we compared anodal and cathodal amplitude values with those obtained in the sham group. The amplitude of N1 component showed non-significant changes with respect to sham values during nor after anodal Cb-tDCS (One-way RM ANOVA or Kruskal-Wallis), but showed a significant increase during cathodal Cb-tDCS (to a maximum of 145.22 ± 6.96 %, N = 5) ($p < 0.01$, One-way ANOVA). Interestingly, these effects were most pronounced at the beginning of Cb-tDCS and decayed over time, even leading to a reversal effect for anodal Cb-tDCS (Fig. 6B). Latency analysis for N1 components showed no significant differences for any of the experimental conditions. Although the One-way RM Analysis of Variance for anodal stimulation was statistically significant ($F_{19,76} = 2.144$, $p = 0.010$), post-hoc tests revealed no significant differences. For cathodal stimulation, the Friedman RM Analysis of Variance on Ranks showed no significant differences ($\chi^2_{19} = 11.578$, $p = 0.903$).

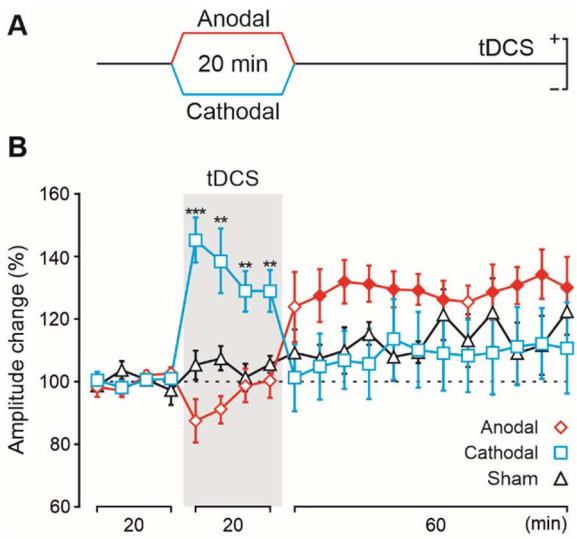

Figure 6. Cb-tDCS after-effects over SEPs in S1. *A*) Illustration of the Cb-tDCS protocol applied for long-term experiments (20 min, 4.26 mA/cm^2). *B*) Normalized amplitude changes of the N1 component of the S1 SEP, averaged every 5 min for 20 min of anodal (red diamonds), cathodal (blue squares), or sham (black triangles) tDCS. Filled symbols indicate statistical differences compared to the last control period (N = 5 mice for anodal, N = 5 for cathodal, N = 8 mice for sham, $p < 0.05$, Holm-Sidak post hoc test). Asterisks indicate statistical differences between the same temporal period for anodal or cathodal Cb-tDCS compared to sham (N = 5 mice for anodal, N = 5 for cathodal, N = 8 mice for sham, *$p < 0.05$; **$p < 0.01$; ***$p < 0.001$, unpaired t-test). Error bars indicate the standard error of the mean (SEM).

Finally, we used antibodies against vGLUT1 and GAD 65-67 to assess possible modifications of the excitation/inhibition balance in S1 after transcranial stimulation of the distant Crus I/II region. A group of animals prepared for Cb-tDCS application during whisker stimulation (no electrophysiological recordings were carried out in this experiment) was randomly assigned to anodal (N = 7), cathodal (N = 7), or sham (N = 7) conditions. Representative confocal images from the control hemisphere on the left and the hemisphere receiving transcranially stimulated cerebellar inputs on the right are presented in Figure 7 for the sham group (at the top), anodal group (in the middle), and cathodal group (at the bottom) for GAD 65-67 (Fig. 7A) and vGLUT1 (Fig. 7B). The number of GAD 65-67 and vGLUT1 positive clusters of puncta in both S1 regions was analyzed as previously. For GAD 65-67, we observed differences in S1 after a single Cb-tDCS session between different Cb-tDCS polarities (2-way mixed ANOVA for GAD 65-67, HEMISPHERE: $F_{1,18}$ =0.007, p = 0.935; POLARITY: $F_{2,18}$ =3.777, p = 0.043; POLARITY x HEMISPHERE: $F_{2,18}$ =2.010, p = 0.163; Fig. 7A). Post hoc analysis revealed a significant decrease in GAD 65-67 levels after anodal Cb-tDCS in the hemisphere ipsilateral to the stimulation (p = 0.014, Bonferroni corrected post hoc test, Fig. 7A). For vGLUT1, no

significant difference was observed in S1 after a single Cb-tDCS session for POLARITY (Kruskal-Wallis, left hemisphere: $\chi^2_2 = 1.415$, $p = 0.493$, right hemisphere: $\chi^2_2 = 1.417$, $p = 0.492$) nor HEMISPHERE (Wilcoxon, anodal: $Z = -1.016$, $p = 0.310$; cathodal: $Z = -0.339$, $p = 0.735$; t-Test, sham: $t_6 = -0.392$, $p = 0.708$; Fig. 7B).

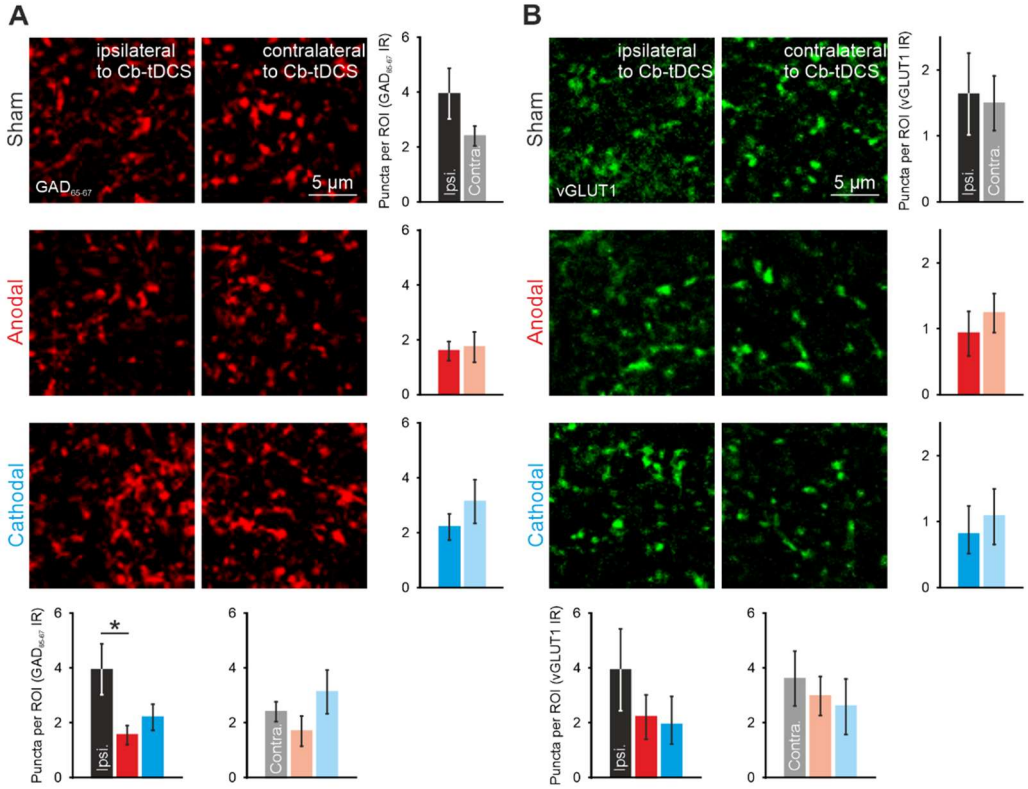

Figure 7. Immunohistochemical immunoreactivity in S1 after 20 minutes of Cb-tDCS. *A,B*) Confocal photomicrographs, quantification, and statistical analysis of GAD 65-67 (*A*) or vGLUT1 immunoreactivity (*B*) in Crus I/II after 20 min of sham condition (upper row, N = 7 mice), anodal Cb-tDCS (middle row, N = 7 mice) and cathodal Cb-tDCS (lower row, N = 7 mice). A comparison of the quantification for the same hemisphere is presented at the bottom. Error bars represent the standard error of the mean (SEM). GAD65-67: Glutamic acid decarboxylase isoforms 65 and 67; vGLUT1: vesicular glutamate transporter 1; ROI: region of interest.

Cb-tDCS elicits changes in the oscillatory properties of S1 but does not affect the stimulated region of the cerebellum

Finally, we calculated the power spectrum ratio values of animals during different time periods, allowing us to compare within and across subjects while accounting for individual variability in baseline power levels. For each animal, the values were extracted, averaged, and referenced to the power obtained during a control period. This normalization technique was useful to minimize the impact of absolute power differences and emphasize the relative

changes in power across different experimental conditions. Spectral power was then calculated for specific frequency bands, including theta (4-10 Hz), beta (10-30 Hz), low-gamma (30-45 Hz), high-gamma (60-100 Hz), HFO1 (100-145 Hz), HFO2 (155-200 Hz), HFO3 (200-245 Hz), and HFO4 (255-300 Hz), for each subject. The average ratios within each group were determined. Additionally, the power bands at 20 minutes (Post1) and 40 minutes (Post2) after Cb-tDCS were compared to the control period for each polarity. In the Crus I/II region after Cb-tDCS (Fig. 8A), no significant differences were observed for any of the analyzed frequency bands. However, in the S1 region, significant differences were found following cathodal Cb-tDCS. Specifically, the power ratio was higher for the Post1 period compared to the control period in low-gamma band (30-45 Hz) (t_6 = 2.716, p = 0.035; one sample t-Test; N = 7), whereas the power ratio was lower in Post2 period compared to the control period in HFO4 band (255-300 Hz) (one sample t-Test, t_6 = -3,147, p = 0.020; N = 7) (Fig. 8B).

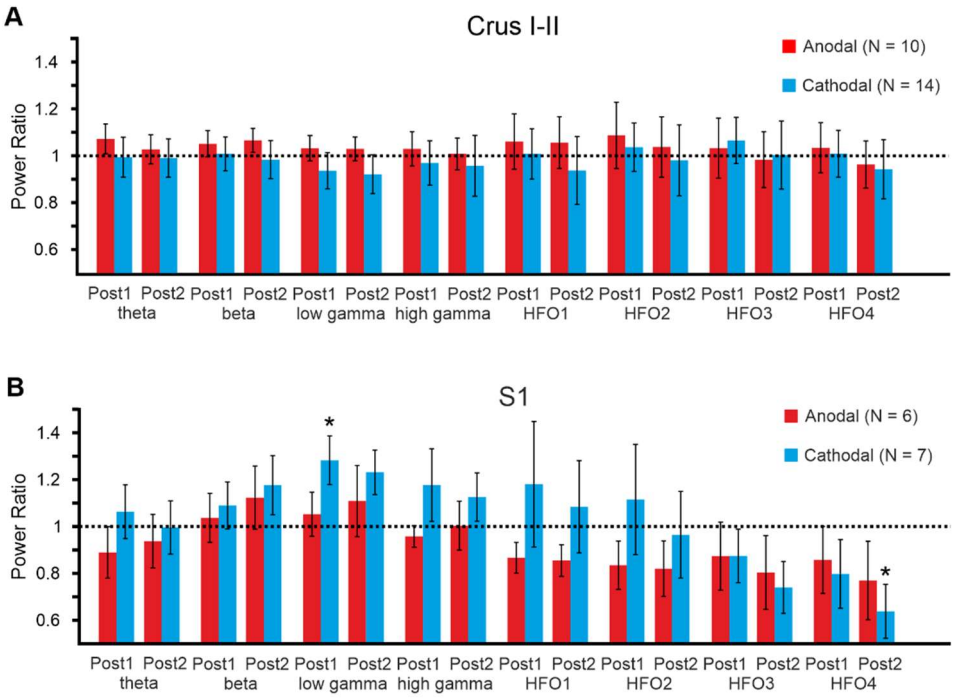

Figure 8. Spectral power analysis of Crus I/II and S1 after Cb-tDCS. Spectral power analysis comparing the power ratio in theta, beta, low gamma, high gamma, HFO1, HFO2, HFO3, and HFO4 bands for different polarities and temporal periods in the Crus I-II (*A*) and S1 (*B*) regions. Power bands from 20 min post-tDCS (Post1) and 40 min post-tDCS (Post2) were compared to the control period. The dashed black line represents the value of the power ratio in the control period. Asterisks show significant differences between time periods (Post1, Post 2) with respect control period (p<0.05 one-sample t-test). Error bars represent the standard error of the mean (SEM). Theta: 4-10 Hz; beta: 10-30 Hz; low gamma: 30-45 Hz; high gamma: 60-100 Hz: HFO1: 100-145 Hz; HFO2: 155-200 Hz; HFO3: 200-245 Hz; HFO4: 255-300 Hz.

Discussion

Cb-tDCS has been shown to modulate neural activity not only within the cerebellar region (Manto et al., 2022) but also in cortical areas (Grimaldi et al., 2016). Therefore, the primary objective of this study was to investigate the impact of Cb-tDCS on both local and distant neuronal excitability. By understanding how Cb-tDCS influences neuronal responses, we should unravel the intricate functional connectivity of the cerebellum, explore its potential therapeutic applications, and advance our comprehension of brain plasticity. This knowledge holds the key to refining treatment approaches for neurological disorders and fostering the development of innovative interventions that enhance brain function. In this study, we sought to investigate the specific effects of Cb-tDCS on SEPs within distinct cerebellar and cortical regions. By doing so, we aimed to uncover valuable insights into the underlying mechanisms and potential clinical implications of cerebellar stimulation.

Characterization of cerebellar SEPs.

The cerebellum receives sensory information from all parts of the body (Garwicz et al., 1998; Apps & Garwicz, 2005) through mossy fibers (Odeh et al., 2005; Jörntell & Ekerot, 2006) and climbing fibers (Ekerot & Jörntell, 2001). Specifically, peripheral stimulation of the whisker pad evokes a sensory potential in CrusI-II lobules of the cerebellar cortex (Brown & Bower, 2002; Lu et al., 2005; Roggeri et al., 2008) that is characterized by two main components (Fig. 1B): the trigeminal (T) component (Armstrong & Drew, 1980; Bower & Woolston, 1983; Morissette & Bower, 1996; Lu et al., 2005; Roggeri et al., 2008) and the cortical (C) component (Sasaki et al., 1969; Brown & Bower, 2002; Mostofi et al., 2010; Diwakar et al., 2011; Parasuram et al., 2018) inputs. Furthermore, the T component consists of N2-N3 waves that reflect the activity between parallel fibers and PC (Márquez-Ruiz & Cheron, 2012). Following prior research, our study demonstrated that electrical stimulation of the whisker elicited a short-latency SEP in the Crus I/II region, exhibiting comparable latency to the findings reported by Márquez-Ruiz and Cheron in 2012. Since the PC are the sole output of the cerebellar cortex, the amplitude of T component can be used as an index of cerebellar cortex excitability. In our experiments, the intensity of whisker stimulation was adjusted to produce a T component with half of the maximum amplitude, ensuring the observation of potential increases as well as decreases in the evoked potentials during and/or after Cb-tDCS.

Local effects of Cb-tDCS.

In 2009, Galea and colleagues (Galea et al., 2009) demonstrated that the connectivity between the cerebellum and M1 can be increased or decreased, depending on the polarity of tDCS applied to human cerebellum. Since then, Cb-tDCS has been used to modulate motor and non-motor behaviors (Grimaldi et al., 2014, 2016; Oldrati & Schutter, 2018), as well as to understand cerebellar functions (Galea et al., 2011; Ferrucci et al., 2012; Boehringer et al., 2013; Miall et al., 2016) and learning mechanisms (Spampinato & Celnik, 2017). In the initial phase of this study, we examined the local effects of Cb-tDCS on Crus I/II by assessing both immediate and long-term impacts on sensory inputs elicited by electrical stimulation of the whiskers.

Regarding immediate effects, we observed that the amplitude of the T component of the SEP was increased during anodal and decreased during cathodal Cb-tDCS. These findings are consistent with previous *in vitro* experiments conducted in isolated turtle cerebellum (Chan & Nicholson, 1986; Chan et al., 1988) and anesthetized rats (Asan et al., 2020), which demonstrated modulation of PC firing rates when DC currents were applied to the cerebellum. Recent research utilizing high-density neuronal recordings in awake mice further highlighted the significance of PC orientation in the ultimate impact of Cb-tDCS, revealing contrasting firing rate modulation in adjacent PC layers with opposite orientations (Sánchez-León et al., 2025). These results suggest that the final effect of Cb-tDCS on a specific region is highly dependent on the anatomical characteristics of the region of interest. In humans, fMRI studies have yielded mixed results in the context of Cb-tDCS effects. For instance, D'Mello and colleagues (D'Mello et al., 2017) observed that anodal Cb-tDCS increased activation in the right Crus I/II during a complex task involving semantic prediction. Additionally, it enhanced resting-state functional connectivity between hubs associated with the task, specifically the reading and language networks. In contrast, no significant differences in cerebellar cortex activity were reported when Cb-tDCS was applied during a simple motor task like finger tapping (Küper et al., 2019). Interestingly, Küper et al. (2019) found the opposite pattern of modulation in the dentate nuclei after Cb-tDCS. They observed increased activation during cathodal stimulation and a trend toward decreased activation during anodal stimulation. These findings align with the inhibitory effect of cathodal Cb-tDCS on the cerebellar cortex, which results in reduced inhibition of the cerebellar nuclei by Purkinje cells,

and vice versa. It is important to note that the electric fields generated during Cb-tDCS in humans are typically below 1 V/m (Parazzini et al., 2014; Fiocchi et al., 2016; Rezaee & Dutta, 2019). This contrasts with rodent studies where electric fields can reach up to 60 V/m (Márquez-Ruiz et al., 2014; Sánchez-León et al., 2025). Therefore, it is crucial to consider the differences in electric field intensities between human and animal studies when interpreting the results and extrapolating findings to clinical applications.

As observed in the immediate-effect results of the cerebellum (Fig. 2B), the cortical C component of the sensory evoked potential (SEP) recorded in Crus I/II exhibited a trend in the opposite direction of modulation compared to the T components. Specifically, anodal Cb-tDCS resulted in a decrease in C component amplitude, while cathodal Cb-tDCS led to a low-increase in amplitude. This observed tendency aligns with our expectations, considering that the cerebellar cortex exerts an inhibitory influence on the cerebral cortex (Batsikadze et al., 2019). Additionally, the C component has been demonstrated to be modulated by activity from S1, as the suppression of S1 activity abolishes the appearance of the C component upon tactile stimulation (Shimuta et al., 2020). Furthermore, diminishing S1 activity lengthens the C component latency, while enhancing S1 activity shortens it (Morissette & Bower, 1996; Brown & Bower, 2002;). According to the hypothesis, increasing cerebellar cortex excitability with anodal Cb-tDCS would decrease activity in the deep cerebellar nuclei (DCN), which project to S1 via the thalamus (Proville et al., 2014). Consequently, this would lead to a decrease in the excitability of S1, which in turn projects back to the cerebellar cortex through the pontine nuclei (Shinoda et al., 1987; Odeh et al., 2005), resulting in a reduction of cortical C component amplitude (Morissette & Bower, 1996; Brown & Bower, 2002). Conversely, when cathodal Cb-tDCS is applied, it is expected to cause an increase in C component amplitude. Notably, a distinct positive deflection was consistently observed between the T and C components, which was reduced during anodal stimulation and enhanced during cathodal stimulation. While our initial quantification of the C component was performed using a peak-to-peak approach, the presence of this intermediate positivity challenges the interpretation of such measures. This intermediate positivity may reflect rebound excitation of DCN following polarity-dependent modulation of PC firing (Person & Raman, 2012). Anodal Cb-tDCS may enhance PC activity and thus increase inhibition of DCN, dampening their excitatory rebound and the associated surface positivity. Conversely, cathodal stimulation may reduce PC firing and disinhibit DCN, enhancing their output. This raises the possibility

that the modulation of this intermediate component—potentially DCN-related—may play a key role in shaping the cerebello-cortical dynamics reflected in the SEP.

Regarding long-term effects after 20 minutes of Cb-tDCS, no modulation was observed for any of the SEP components in Crus I/II. Throughout the 20 minutes of stimulation, the immediate modulation persisted, showing a robust effect on the amplitude of the trigeminal T component, which increased with anodal stimulation and decreased with cathodal stimulation. However, once the Cb-tDCS was discontinued, all amplitude values returned to their respective control values. Similar effects have been demonstrated in fMRI studies involving human participants (Küper et al., 2019), where no significant difference in cerebellar cortical activation was observed following Cb-tDCS. Another study involving a cerebellar-dependent semantic prediction task during Cb-tDCS reported that anodal stimulation led to an increase in activity in CrusI/II, along with enhanced functional connectivity between the task-related hubs (D'Mello et al., 2017). However, human studies utilizing Cb-tDCS often rely on indirect measurements of cerebellar excitability, such as behavioral outcomes or the excitability of connected regions. In these cases, contradictory results are frequently observed (Pope & Miall, 2012; Zuchowski et al., 2014; Miall et al., 2016; Beyer et al., 2017; Batsikadze et al., 2019). There could be several reasons for this disparity, including variations in the orientation of neurons in different cerebellar areas relative to the applied electric field (Grimaldi et al., 2016; Sánchez-León et al., 2023). Furthermore, cerebellar modulation might distinctly affect distantly interconnected regions (Stagg et al., 2018; Miterko et al., 2019). Additionally, present results underscore the importance of conducting experimental measurements and potential behavioral tasks during the administration of Cb-tDCS rather than afterward. Even with significantly higher electric fields employed in our experiments, no long-term effects were observed in the cerebellar cortex. Currently, there is evidence supporting the significance of this assumption, as several studies have demonstrated that anodal tDCS applied over the cerebellum enhances skill learning compared to sham stimulation, specifically by augmenting online learning (during Cb-tDCS) rather than offline learning (after Cb-tDCS) (Cantarero et al., 2015). Moreover, these studies have highlighted the relevance of the cerebellum during the early phases of motor skill learning (Spampinato & Celnik, 2017) or in visuomotor adaptation tasks (Galea et al., 2011). Consistent with the electrophysiological findings, our immunohistochemical analysis of GAD65-67 and vGlut1 immunoreactivity levels in Crus I/II revealed no changes following 20 minutes of Cb-tDCS. This

lack of alteration in neurotransmitter levels after Cb-tDCS has also been observed in human experiments utilizing magnetic resonance spectroscopy (MRS) to measure GABA and glutamate levels (Jalali et al., 2018). However, they also did not find any differences during Cb-tDCS, suggesting that the immediate effects of tDCS on the cerebellar cortex might be confined to the polarization induced by the electric field and not correlated with changes in neurotransmitter levels.

Distant effects of Cb-tDCS.

S1 exhibits a high degree of interconnectivity with the cerebellum, as demonstrated by previous studies (Schmahmann, 2001; Ramnani, 2006; Buckner et al., 2011). The extensive characterization of these projections has been achieved through both anatomical investigations (Leergaard et al., 2000) and functional studies (Allen et al., 1979; Shinoda et al., 1987; Swenson et al., 1989; Morissette & Bower, 1996; Brown & Bower, 2002; Nagao, 2004; Odeh et al., 2005; Watson et al., 2009). However, it is only recently that the details and significance of this connection have begun to be elucidated (Proville et al., 2014; Caligiore et al., 2017; Bostan & Strick, 2018). In the present study, the immediate effects of Cb-tDCS on S1 excitability showed a decrease in N1 amplitude during anodal stimulation and an increase during cathodal stimulation, contrasting with the effects observed in the Crus I/II region. In line with these findings, a previous animal study demonstrated that manipulating the activity of the posterior cerebellar cortex (Crus I) using chemogenetic techniques resulted in a decrease or increase in the firing rate of neurons in the contralateral parietal association cortex, depending on whether PC activity was increased or decreased, respectively (Stoodley et al., 2017). Furthermore, human studies utilizing indirect measurements have shown that cathodal Cb-tDCS leads to a decrease in the inhibitory influence exerted by the cerebellum on the primary motor cortex (M1), whereas anodal Cb-tDCS has been found to increase this inhibition (Galea et al., 2009; Batsikadze et al., 2019).

In the context of the long-term effects of Cb-tDCS experiments, it was observed that cathodal Cb-tDCS led to an increase in the amplitude of SEPs recorded in S1 during the application of Cb-tDCS, but no long-term effects were observed after Cb-tDCS cessation. On the other hand, anodal Cb-tDCS initially decreased the excitability of S1, but this effect was abolished after several minutes (Fig. 6B). Interestingly, when anodal Cb-tDCS was turned off, a rebound effect was observed in the amplitude of S1-SEPs, indicating a rapid increase in excitability that

persisted for at least 1 hour. This rebound increase in amplitude could be attributed to homeostatic mechanisms that balance overall excitability. Supporting these findings, a previous animal study conducted by Proville and colleagues (Proville et al., 2014) demonstrated that optogenetic stimulation of the Crus I area led to an initial inhibition followed by a subsequent rebound activation of the cerebello-thalamo-cortical pathway, resulting in the activation of the primary motor cortex (M1). However, it is noteworthy that the observed rebound effect was not evident in our recordings from CrusI-II during Cb-tDCS (Fig. 3B). This suggests that the mechanism responsible for the rebound effect may reside in another brain region, such as the thalamus or S1. The immunohistochemical analysis conducted on S1 revealed a significant reduction in the immunoreactivity levels of GAD65-67 following ipsilateral anodal Cb-tDCS. This measurement is in agreement with the long-lasting increase in excitability observed in the SEPs after anodal Cb-tDCS, suggesting a decrease in S1 GABA levels as a possible mechanism. A decrease in GABA after the administration of anodal tDCS over the same area of analysis has been proven in humans (Nandi et al., 2022) and animal (Zhao et al., 2020) studies, but to the extent of our knowledge this is the first evidence that the stimulation of a distant area can not only modulate the excitability but also the neurotransmitters levels of another interconnected region of the brain.

Taken together, these findings provide compelling evidence regarding the distal effects of Cb-tDCS. The results suggest that the effects of non-invasive neuromodulation are not confined to the stimulated region but can extend throughout the entire network (Stagg et al., 2018). This has important implications for both current (Pope & Miall, 2012; Yosephi et al., 2018; Marron et al., 2019) and future (Stoodley et al., 2017; Menardy et al., 2019) therapies that aim to modulate cerebellar networks. These findings highlight the potential utility of targeting the cerebellum for neuromodulatory interventions, as its effects can influence the broader neural network.

Impact of Cb-tDCS on local and distant oscillatory activities.

Numerous human studies have demonstrated the crucial involvement of oscillatory brain activity in the formation of perceptions and memory, highlighting its essential role in perceptual and behavioral functions (Engel & Singer, 2001). The present study demonstrated significant differences in the power spectrum ratio of the S1 region following cathodal Cb-

tDCS. Specifically, a higher power ratio was observed in the low-gamma band (30-45 Hz), while a lower power ratio was observed in the high-frequency oscillation (HFO) band (255-300 Hz) compared to the control period. Interestingly, low-gamma band oscillation accompanied the early somatosensory evoked potentials in humans (Cheron et al., 2007). However, no significant differences were found in the Crus I/II region for any of the analyzed frequency bands. Like the results obtained for the S1-SEPs induced by whisker stimulation, these findings once again confirm the presence of distant rather than local long-term effects following Cb-tDCS.

Gamma oscillations have been implicated in various cognitive processes, including visual attention (Engel & Singer, 2001), encoding, retention, and retrieval of information across sensory modalities (Tallon-Baudry & Bertrand, 1999; Herrmann et al., 2004; Kahana, 2006), as well as sensory perception (Siegle et al., 2014). Gamma band changes have been previously associated with local effects of cathodal tDCS. Antal and colleagues (2004) demonstrated that cathodal tDCS applied to the occipital cortex in humans decreased gamma frequency power. Consistently, our previous research showed that direct cathodal tDCS applied to the S1 area of awake mice resulted in a reduction in gamma band power, while anodal tDCS did not induce significant changes (Sánchez-León et al., 2021). The enhancement of cortical gamma activity observed in this study following Cb-tDCS could have therapeutic implications for conditions characterized by abnormal gamma oscillations, such as Alzheimer's Disease (Casula et al., 2022), schizophrenia (Hirano et al., 2015), autism spectrum disorders (Kayarian et al., 2020), major depression (Fitzgerald & Watson, 2018) or epilepsy (Hughes, 2008). Interestingly, high-frequency oscillations (HFOs) have been observed in diverse brain structures (Jones & Barth, 1999; Amassian & Stewart, 2003; Traub & Whittington, 2010; Uhlhaas & Singer, 2015) during pathological conditions such as seizures (Alkawadri et al., 2014; Frauscher et al., 2017). The reduction in the upper HFO band (255-300 Hz) observed in the present study supports the potential application of cathodal Cb-tDCS in exploring fundamental cognitive processes and treating various pathological states. However, it is important to note that HFOs are not solely restricted to pathological processes but can also manifest in normal contexts like cognition and sleep (Buzsáki et al., 1992; Chrobak & Buzsáki, 1996).

In conclusion, the study provides compelling evidence that Cb-tDCS effectively modulates the amplitude of SEPs in both the cerebellum and S1. Notably, immediate opposite

effects were observed during the application of Cb-tDCS, suggesting a bidirectional influence. On the other hand, long-term effects were found to extend primarily to distant regions, indicating a more distributed neural impact. These findings significantly advance our understanding of the neural mechanisms underlying Cb-tDCS and its potential for modulating cerebellar-brain interactions.

Author contributions

C.A.S-L and J.M-R conceived the original idea and designed the experiments. C.A.S-L, I.C, A.J-D and J.M-R performed the experiments and the data analysis. C.A.S-L and J.M-R wrote the paper. G.C and J.F.M assisted in the experimental design and in the interpretation of the results. All the authors contributed to the final edition of the manuscript.

References

Alkawadri, R., Gaspard, N., Goncharova, I. I., Spencer, D. D., Gerrard, J. L., Zaveri, H., Duckrow, R. B., Blumenfeld, H., & Hirsch, L. J. (2014). The spatial and signal characteristics of physiologic high frequency oscillations. *Epilepsia*, *55*(12), 1986–1995. https://doi.org/10.1111/epi.12851

Allen, G. I., Azzena, G. B., & Ohno, T. (1979). Pontine and non-pontine pathways mediating early mossy fiber responses from sensorimotor cortex to cerebellum in the cat. *Experimental Brain Research*, *36*(2), 359–374. https://doi.org/10.1007/BF00238917

Amassian, V. E., & Stewart, M. (2003). Motor cortical and other cortical interneuronal networks that generate very high frequency waves. *Supplements to Clinical Neurophysiology*, *56*, 119–142. https://doi.org/10.1016/s1567-424x(09)70214-4

Antal, A., Kincses, T. Z., Nitsche, M. A., Bartfai, O., & Paulus, W. (2004). Excitability changes induced in the human primary visual cortex by transcranial direct current stimulation: Direct electrophysiological evidence. *Investigative Ophthalmology & Visual Science*, *45*(2), 702–707. https://doi.org/10.1167/iovs.03-0688

Apps, R., & Garwicz, M. (2005). Anatomical and physiological foundations of cerebellar information processing. *Nature Reviews. Neuroscience*, *6*(4). https://doi.org/10.1038/nrn1646

Armstrong, D. M., & Drew, T. (1980). Responses in the posterior lobe of the rat cerebellum to electrical stimulation of cutaneous afferents to the snout. *The Journal of Physiology*, *309*, 357–374. https://doi.org/10.1113/jphysiol.1980.sp013513

Asan, A. S., Lang, E. J., & Sahin, M. (2020). Entrainment of cerebellar purkinje cells with directional AC electric fields in anesthetized rats. *Brain Stimulation*, *13*(6), 1548–1558. https://doi.org/10.1016/j.brs.2020.08.017

Bastiaansen, M., & Hagoort, P. (2003). Event-induced theta responses as a window on the dynamics of memory. *Cortex; a Journal Devoted to the Study of the Nervous System and Behavior*, *39*(4–5), 967–992. https://doi.org/10.1016/s0010-9452(08)70873-6

Batsikadze, G., Rezaee, Z., Chang, D.-I., Gerwig, M., Herlitze, S., Dutta, A., Nitsche, M. A., & Timmann, D. (2019). Effects of cerebellar transcranial direct current stimulation on cerebellar-brain inhibition in humans: A systematic evaluation. *Brain Stimulation*, *12*(5), 1177–1186. https://doi.org/10.1016/j.brs.2019.04.010

Baumann, O., Borra, R. J., Bower, J. M., Cullen, K. E., Habas, C., Ivry, R. B., Leggio, M., Mattingley, J. B., Molinari, M., Moulton, E. A., Paulin, M. G., Pavlova, M. A., Schmahmann, J. D., & Sokolov, A. A. (2015). Consensus paper: The role of the cerebellum in perceptual processes. *Cerebellum (London, England)*, *14*(2), 197–220. https://doi.org/10.1007/s12311-014-0627-7

Beyer, L., Batsikadze, G., Timmann, D., & Gerwig, M. (2017). Cerebellar tDCS Effects on Conditioned Eyeblinks using Different Electrode Placements and Stimulation Protocols. *Frontiers in Human Neuroscience*, *11*, 23. https://doi.org/10.3389/fnhum.2017.00023

Boehringer, A., Macher, K., Dukart, J., Villringer, A., & Pleger, B. (2013). Cerebellar transcranial direct current stimulation modulates verbal working memory. *Brain Stimulation*, *6*(4), 649–653. https://doi.org/10.1016/j.brs.2012.10.001

Bostan, A. C., Dum, R. P., & Strick, P. L. (2013). Cerebellar networks with the cerebral cortex and basal ganglia. *Trends in Cognitive Sciences*, *17*(5), 241–254. https://doi.org/10.1016/j.tics.2013.03.003

Bostan, A. C., & Strick, P. L. (2018). The basal ganglia and the cerebellum: Nodes in an integrated network. *Nature Reviews. Neuroscience*, *19*(6), 338–350. https://doi.org/10.1038/s41583-018-0002-7

Bower, J. M., & Woolston, D. C. (1983). Congruence of spatial organization of tactile projections to granule cell and Purkinje cell layers of cerebellar hemispheres of the albino rat: Vertical organization of cerebellar cortex. *Journal of Neurophysiology*, *49*(3), 745–766. https://doi.org/10.1152/jn.1983.49.3.745

Brown, I. E., & Bower, J. M. (2002). The influence of somatosensory cortex on climbing fiber responses in the lateral hemispheres of the rat cerebellum after peripheral tactile stimulation. *The Journal of Neuroscience: The Official Journal of the Society for Neuroscience*, *22*(15), 6819–6829. https://doi.org/10.1523/JNEUROSCI.22-15-06819.2002

Buckner, R. L., Krienen, F. M., Castellanos, A., Diaz, J. C., & Yeo, B. T. T. (2011). The organization of the human cerebellum estimated by intrinsic functional connectivity. *Journal of Neurophysiology*, *106*(5), 2322–2345. https://doi.org/10.1152/jn.00339.2011

Buzsáki, G., Horváth, Z., Urioste, R., Hetke, J., & Wise, K. (1992). High-frequency network oscillation in the hippocampus. *Science (New York, N.Y.)*, *256*(5059), 1025–1027. https://doi.org/10.1126/science.1589772

Caligiore, D., Pezzulo, G., Baldassarre, G., Bostan, A. C., Strick, P. L., Doya, K., Helmich, R. C., Dirkx, M., Houk, J., Jörntell, H., Lago-Rodriguez, A., Galea, J. M., Miall, R. C., Popa, T., Kishore, A., Verschure, P. F. M. J., Zucca, R., & Herreros, I. (2017). Consensus Paper: Towards a Systems-Level View of Cerebellar Function: the Interplay Between Cerebellum, Basal Ganglia, and Cortex. *Cerebellum (London, England)*, *16*(1), 203–229. https://doi.org/10.1007/s12311-016-0763-3

Cantarero, G., Spampinato, D., Reis, J., Ajagbe, L., Thompson, T., Kulkarni, K., & Celnik, P. (2015). Cerebellar direct current stimulation enhances on-line motor skill acquisition through an effect on accuracy. *The Journal of Neuroscience: The Official Journal of the Society for Neuroscience*, *35*(7), 3285–3290. https://doi.org/10.1523/JNEUROSCI.2885-14.2015

Castro-Alamancos, M. A., & Bezdudnaya, T. (2015). Modulation of artificial whisking related signals in barrel cortex. *Journal of Neurophysiology*, *113*(5), 1287–1301. https://doi.org/10.1152/jn.00809.2014

Casula, E. P., Pellicciari, M. C., Bonnì, S., Borghi, I., Maiella, M., Assogna, M., Minei, M., Motta, C., D'Acunto, A., Porrazzini, F., Pezzopane, V., Mencarelli, L., Roncaioli, A., Rocchi, L., Spampinato, D. A., Caltagirone, C., Santarnecchi, E., Martorana, A., & Koch, G. (2022). Decreased Frontal Gamma Activity in Alzheimer Disease Patients. *Annals of Neurology*, *92*(3), 464–475. https://doi.org/10.1002/ana.26444

Chan, C. Y., Hounsgaard, J., & Nicholson, C. (1988). Effects of electric fields on transmembrane potential and excitability of turtle cerebellar Purkinje cells in vitro. *The Journal of Physiology*, *402*, 751–771. https://doi.org/10.1113/jphysiol.1988.sp017232

Chan, C. Y., & Nicholson, C. (1986). Modulation by applied electric fields of Purkinje and stellate cell activity in the isolated turtle cerebellum. *The Journal of Physiology*, *371*, 89–114. https://doi.org/10.1113/jphysiol.1986.sp015963

Cheron, G., Cebolla, A. M., De Saedeleer, C., Bengoetxea, A., Leurs, F., Leroy, A., & Dan, B. (2007). Pure phase-locking of beta/gamma oscillation contributes to the N30 frontal component of somatosensory evoked potentials. *BMC neuroscience, 8,* 75. https://doi.org/10.1186/1471-2202-8-75

Chrobak, J. J., & Buzsáki, G. (1996). High-frequency oscillations in the output networks of the hippocampal-entorhinal axis of the freely behaving rat. *The Journal of Neuroscience: The Official Journal of the Society for Neuroscience*, *16*(9), 3056–3066. https://doi.org/10.1523/JNEUROSCI.16-09-03056.1996

Dieckhöfer, A., Waberski, T. D., Nitsche, M., Paulus, W., Buchner, H., & Gobbelé, R. (2006). Transcranial direct current stimulation applied over the somatosensory cortex—Differential effect on low and high frequency SEPs. *Clinical Neurophysiology: Official Journal of the International Federation of Clinical Neurophysiology*, *117*(10), 2221–2227. https://doi.org/10.1016/j.clinph.2006.07.136

Diwakar, S., Lombardo, P., Solinas, S., Naldi, G., & D'Angelo, E. (2011). Local field potential modeling predicts dense activation in cerebellar granule cells clusters under LTP and LTD control. *PloS One*, *6*(7), e21928. https://doi.org/10.1371/journal.pone.0021928

D'Mello, A. M., Turkeltaub, P. E., & Stoodley, C. J. (2017). Cerebellar tDCS Modulates Neural Circuits during Semantic Prediction: A Combined tDCS-fMRI Study. *The Journal of Neuroscience: The Official Journal of the Society for Neuroscience*, *37*(6), 1604–1613. https://doi.org/10.1523/JNEUROSCI.2818-16.2017

Ekerot, C. F., & Jörntell, H. (2001). Parallel fibre receptive fields of Purkinje cells and interneurons are climbing fibre-specific. *The European Journal of Neuroscience*, *13*(7), 1303–1310. https://doi.org/10.1046/j.0953-816x.2001.01499.x

Engel, A. K., & Singer, W. (2001). Temporal binding and the neural correlates of sensory awareness. *Trends in Cognitive Sciences*, *5*(1), 16–25. https://doi.org/10.1016/s1364-6613(00)01568-0

Fernández, M., Sánchez-León, C. A., Llorente, J., Sierra-Arregui, T., Knafo, S., Márquez-Ruiz, J., & Peñagarikano, O. (2021). Altered Cerebellar Response to Somatosensory Stimuli in the Cntnap2 Mouse Model of Autism. *ENeuro*, *8*(5), ENEURO.0333-21.2021. https://doi.org/10.1523/ENEURO.0333-21.2021

Ferrucci, R., Giannicola, G., Rosa, M., Fumagalli, M., Boggio, P. S., Hallett, M., Zago, S., & Priori, A. (2012). Cerebellum and processing of negative facial emotions: Cerebellar transcranial DC stimulation specifically enhances the emotional recognition of facial anger and sadness. *Cognition & Emotion*, *26*(5), 786–799. https://doi.org/10.1080/02699931.2011.619520

Fiocchi, S., Ravazzani, P., Priori, A., & Parazzini, M. (2016). Cerebellar and Spinal Direct Current Stimulation in Children: Computational Modeling of the Induced Electric Field. *Frontiers in Human Neuroscience*, *10*, 522. https://doi.org/10.3389/fnhum.2016.00522

Fitzgerald, P. J., & Watson, B. O. (2018). Gamma oscillations as a biomarker for major depression: An emerging topic. *Translational Psychiatry*, *8*(1), 177. https://doi.org/10.1038/s41398-018-0239-y

Frauscher, B., Bartolomei, F., Kobayashi, K., Cimbalnik, J., van 't Klooster, M. A., Rampp, S., Otsubo, H., Höller, Y., Wu, J. Y., Asano, E., Engel, J., Kahane, P., Jacobs, J., & Gotman, J. (2017). High-frequency oscillations: The state of clinical research. *Epilepsia*, *58*(8), 1316–1329. https://doi.org/10.1111/epi.13829

Galea, J. M., Jayaram, G., Ajagbe, L., & Celnik, P. (2009). Modulation of cerebellar excitability by polarity-specific noninvasive direct current stimulation. *The Journal of*

Neuroscience: The Official Journal of the Society for Neuroscience, *29*(28), 9115–9122. https://doi.org/10.1523/JNEUROSCI.2184-09.2009

Galea, J. M., Vazquez, A., Pasricha, N., de Xivry, J.-J. O., & Celnik, P. (2011). Dissociating the roles of the cerebellum and motor cortex during adaptive learning: The motor cortex retains what the cerebellum learns. *Cerebral Cortex (New York, N.Y.: 1991)*, *21*(8), 1761–1770. https://doi.org/10.1093/cercor/bhq246

Garwicz, M., Ekerot, C.-F., & Jörntell, H. (1998). Organizational Principles of Cerebellar Neuronal Circuitry. *News in Physiological Sciences: An International Journal of Physiology Produced Jointly by the International Union of Physiological Sciences and the American Physiological Society*, *13*, 26–32. https://doi.org/10.1152/physiologyonline.1998.13.1.26

Gornati, S. V., Schäfer, C. B., Eelkman Rooda, O. H. J., Nigg, A. L., De Zeeuw, C. I., & Hoebeek, F. E. (2018). Differentiating Cerebellar Impact on Thalamic Nuclei. *Cell Reports*, *23*(9), 2690–2704. https://doi.org/10.1016/j.celrep.2018.04.098

Grimaldi, G., Argyropoulos, G. P., Bastian, A., Cortes, M., Davis, N. J., Edwards, D. J., Ferrucci, R., Fregni, F., Galea, J. M., Hamada, M., Manto, M., Miall, R. C., Morales-Quezada, L., Pope, P. A., Priori, A., Rothwell, J., Tomlinson, S. P., & Celnik, P. (2016). Cerebellar Transcranial Direct Current Stimulation (ctDCS): A Novel Approach to Understanding Cerebellar Function in Health and Disease. *The Neuroscientist: A Review Journal Bringing Neurobiology, Neurology and Psychiatry*, *22*(1), 83–97. https://doi.org/10.1177/1073858414559409

Grimaldi, G., Argyropoulos, G. P., Boehringer, A., Celnik, P., Edwards, M. J., Ferrucci, R., Galea, J. M., Groiss, S. J., Hiraoka, K., Kassavetis, P., Lesage, E., Manto, M., Miall, R. C., Priori, A., Sadnicka, A., Ugawa, Y., & Ziemann, U. (2014). Non-invasive cerebellar stimulation—A consensus paper. *Cerebellum (London, England)*, *13*(1), 121–138. https://doi.org/10.1007/s12311-013-0514-7

Herrmann, C. S., Senkowski, D., & Röttger, S. (2004). Phase-locking and amplitude modulations of EEG alpha: Two measures reflect different cognitive processes in a working memory task. *Experimental Psychology*, *51*(4), 311–318. https://doi.org/10.1027/1618-3169.51.4.311

Hirano, Y., Oribe, N., Kanba, S., Onitsuka, T., Nestor, P. G., & Spencer, K. M. (2015). Spontaneous Gamma Activity in Schizophrenia. *JAMA Psychiatry*, *72*(8), 813–821. https://doi.org/10.1001/jamapsychiatry.2014.2642

Hughes, J. R. (2008). Gamma, fast, and ultrafast waves of the brain: Their relationships with epilepsy and behavior. *Epilepsy & Behavior: E&B*, *13*(1), 25–31. https://doi.org/10.1016/j.yebeh.2008.01.011

Ito, M. (2002). Historical review of the significance of the cerebellum and the role of Purkinje cells in motor learning. *Annals of the New York Academy of Sciences*, *978*, 273–288. https://doi.org/10.1111/j.1749-6632.2002.tb07574.x

Jalali, R., Chowdhury, A., Wilson, M., Miall, R. C., & Galea, J. M. (2018). Neural changes associated with cerebellar tDCS studied using MR spectroscopy. *Experimental Brain Research*, *236*(4), 997–1006. https://doi.org/10.1007/s00221-018-5170-1

Jones, M. S., & Barth, D. S. (1999). Spatiotemporal organization of fast (>200 Hz) electrical oscillations in rat Vibrissa/Barrel cortex. *Journal of Neurophysiology*, *82*(3), 1599–1609. https://doi.org/10.1152/jn.1999.82.3.1599

Jörntell, H., & Ekerot, C.-F. (2006). Properties of somatosensory synaptic integration in cerebellar granule cells in vivo. *The Journal of Neuroscience: The Official Journal of the Society for Neuroscience*, *26*(45), 11786–11797. https://doi.org/10.1523/JNEUROSCI.2939-06.2006

Kahana, M. J. (2006). The cognitive correlates of human brain oscillations. *The Journal of Neuroscience: The Official Journal of the Society for Neuroscience*, *26*(6), 1669–1672. https://doi.org/10.1523/JNEUROSCI.3737-05c.2006

Kayarian, F. B., Jannati, A., Rotenberg, A., & Santarnecchi, E. (2020). Targeting Gamma-Related Pathophysiology in Autism Spectrum Disorder Using Transcranial Electrical Stimulation: Opportunities and Challenges. *Autism Research: Official Journal of the International Society for Autism Research*, *13*(7), 1051–1071. https://doi.org/10.1002/aur.2312

Küper, M., Mallick, J. S., Ernst, T., Kraff, O., Thürling, M., Stefanescu, M. R., Göricke, S., Nitsche, M. A., & Timmann, D. (2019). Cerebellar transcranial direct current stimulation modulates the fMRI signal in the cerebellar nuclei in a simple motor task. *Brain Stimulation*, *12*(5), 1169–1176. https://doi.org/10.1016/j.brs.2019.04.002

Lawrenson, C. L., Watson, T. C., & Apps, R. (2016). Transmission of Predictable Sensory Signals to the Cerebellum via Climbing Fiber Pathways Is Gated during Exploratory Behavior. *The Journal of Neuroscience: The Official Journal of the Society for Neuroscience*, *36*(30), 7841–7851. https://doi.org/10.1523/JNEUROSCI.0439-16.2016

Leergaard, T. B., Lyngstad, K. A., Thompson, J. H., Taeymans, S., Vos, B. P., De Schutter, E., Bower, J. M., & Bjaalie, J. G. (2000). Rat somatosensory cerebropontocerebellar pathways: Spatial relationships of the somatotopic map of the primary somatosensory cortex are preserved in a three-dimensional clustered pontine map. *The Journal of Comparative Neurology*, *422*(2), 246–266. https://doi.org/10.1002/(sici)1096-9861(20000626)422:2<246::aid-cne7>3.0.co;2-r

Lu, H., Hartmann, M. J., & Bower, J. M. (2005). Correlations between purkinje cell single-unit activity and simultaneously recorded field potentials in the immediately underlying granule cell layer. *Journal of Neurophysiology*, *94*(3), 1849–1860. https://doi.org/10.1152/jn.01275.2004

Manto, M., Argyropoulos, G. P. D., Bocci, T., Celnik, P. A., Corben, L. A., Guidetti, M., Koch, G., Priori, A., Rothwell, J. C., Sadnicka, A., Spampinato, D., Ugawa, Y., Wessel, M. J., & Ferrucci, R. (2022). Consensus Paper: Novel Directions and Next Steps of Non-invasive Brain Stimulation of the Cerebellum in Health and Disease. *Cerebellum (London, England)*, *21*(6), 1092–1122. https://doi.org/10.1007/s12311-021-01344-6

Mapelli, J., & D'Angelo, E. (2007). The spatial organization of long-term synaptic plasticity at the input stage of cerebellum. *The Journal of Neuroscience: The Official Journal of the Society for Neuroscience*, *27*(6), 1285–1296. https://doi.org/10.1523/JNEUROSCI.4873-06.2007

Márquez-Ruiz, J., & Cheron, G. (2012). Sensory stimulation-dependent plasticity in the cerebellar cortex of alert mice. *PloS One*, *7*(4), e36184. https://doi.org/10.1371/journal.pone.0036184

Márquez-Ruiz, J., Leal-Campanario, R., Sánchez-Campusano, R., Molaee-Ardekani, B., Wendling, F., Miranda, P. C., Ruffini, G., Gruart, A., & Delgado-García, J. M. (2012). Transcranial direct-current stimulation modulates synaptic mechanisms involved in associative learning in behaving rabbits. *Proceedings of the National Academy of Sciences of the United States of America*, *109*(17), 6710–6715. https://doi.org/10.1073/pnas.1121147109

Márquez-Ruiz, J., Leal-Campanario, R., Wendling, F., Ruffini, G., Gruart, A., & Delgado-García, J. (2014). Transcranial Electrical Stimulation in Animals. In *The Stimulated Brain: Cognitive Enhancement Using Non-Invasive Brain Stimulation* (pp. 117–144). https://doi.org/10.1016/B978-0-12-404704-4.00005-3

Marron, E. M., Viejo-Sobera, R., Cuatrecasas, G., Redolar-Ripoll, D., Lorda, P. G., Datta, A., Bikson, M., Magerowski, G., & Alonso-Alonso, M. (2019). Prefronto-cerebellar neuromodulation affects appetite in obesity. *International Journal of Obesity (2005)*, *43*(10), 2119–2124. https://doi.org/10.1038/s41366-018-0278-8

Matsunaga, K., Nitsche, M. A., Tsuji, S., & Rothwell, J. C. (2004). Effect of transcranial DC sensorimotor cortex stimulation on somatosensory evoked potentials in humans. *Clinical Neurophysiology: Official Journal of the International Federation of Clinical Neurophysiology*, *115*(2), 456–460. https://doi.org/10.1016/s1388-2457(03)00362-6

Menardy, F., Varani, A. P., Combes, A., Léna, C., & Popa, D. (2019). Functional Alteration of Cerebello-Cerebral Coupling in an Experimental Mouse Model of Parkinson's Disease. *Cerebral Cortex (New York, N.Y.: 1991)*, *29*(4), 1752–1766. https://doi.org/10.1093/cercor/bhy346

Miall, R. C., Antony, J., Goldsmith-Sumner, A., Harding, S. R., McGovern, C., & Winter, J. L. (2016). Modulation of linguistic prediction by TDCS of the right lateral cerebellum. *Neuropsychologia*, *86*, 103–109. https://doi.org/10.1016/j.neuropsychologia.2016.04.022

Miterko, L. N., Baker, K. B., Beckinghausen, J., Bradnam, L. V., Cheng, M. Y., Cooperrider, J., DeLong, M. R., Gornati, S. V., Hallett, M., Heck, D. H., Hoebeek, F. E., Kouzani, A. Z., Kuo, S.-H., Louis, E. D., Machado, A., Manto, M., McCambridge, A. B., Nitsche, M. A., Taib, N. O. B., … Sillitoe, R. V. (2019). Consensus Paper: Experimental Neurostimulation of the Cerebellum. *Cerebellum (London, England)*, *18*(6), 1064–1097. https://doi.org/10.1007/s12311-019-01041-5

Morissette, J., & Bower, J. M. (1996). Contribution of somatosensory cortex to responses in the rat cerebellar granule cell layer following peripheral tactile stimulation. *Experimental Brain Research*, *109*(2), 240–250. https://doi.org/10.1007/BF00231784

Mostofi, A., Holtzman, T., Grout, A. S., Yeo, C. H., & Edgley, S. A. (2010). Electrophysiological localization of eyeblink-related microzones in rabbit cerebellar cortex. *The Journal of*

Neuroscience: The Official Journal of the Society for Neuroscience, *30*(26), 8920–8934. https://doi.org/10.1523/JNEUROSCI.6117-09.2010

Nagao, S. (2004). Pontine nuclei-mediated cerebello-cerebral interactions and its functional role. *Cerebellum (London, England)*, *3*(1), 11–15. https://doi.org/10.1080/14734220310012181

Nandi, T., Puonti, O., Clarke, W. T., Nettekoven, C., Barron, H. C., Kolasinski, J., Hanayik, T., Hinson, E. L., Berrington, A., Bachtiar, V., Johnstone, A., Winkler, A. M., Thielscher, A., Johansen-Berg, H., & Stagg, C. J. (2022). TDCS induced GABA change is associated with the simulated electric field in M1, an effect mediated by grey matter volume in the MRS voxel. *Brain Stimulation*, *15*(5), 1153–1162. https://doi.org/10.1016/j.brs.2022.07.049

Nitsche, M. A., & Paulus, W. (2000). Excitability changes induced in the human motor cortex by weak transcranial direct current stimulation. *The Journal of Physiology*, *527 Pt 3*(Pt 3), 633–639. https://doi.org/10.1111/j.1469-7793.2000.t01-1-00633.x

Odeh, F., Ackerley, R., Bjaalie, J. G., & Apps, R. (2005). Pontine maps linking somatosensory and cerebellar cortices are in register with climbing fiber somatotopy. *The Journal of Neuroscience: The Official Journal of the Society for Neuroscience*, *25*(24), 5680–5690. https://doi.org/10.1523/JNEUROSCI.0558-05.2005

Oldrati, V., & Schutter, D. J. L. G. (2018). Targeting the Human Cerebellum with Transcranial Direct Current Stimulation to Modulate Behavior: A Meta-Analysis. *Cerebellum (London, England)*, *17*(2), 228–236. https://doi.org/10.1007/s12311-017-0877-2

Oostenveld, R., Fries, P., Maris, E., & Schoffelen, J.-M. (2011). FieldTrip: Open source software for advanced analysis of MEG, EEG, and invasive electrophysiological data. *Computational Intelligence and Neuroscience*, *2011*, 156869. https://doi.org/10.1155/2011/156869

Parasuram, H., Nair, B., Naldi, G., D'Angelo, E., & Diwakar, S. (2018). Understanding Cerebellum Granular Layer Network Computations through Mathematical Reconstructions of Evoked Local Field Potentials. *Annals of Neurosciences*, *25*(1), 11–24. https://doi.org/10.1159/000481905

Parazzini, M., Rossi, E., Ferrucci, R., Liorni, I., Priori, A., & Ravazzani, P. (2014). Modelling the electric field and the current density generated by cerebellar transcranial DC stimulation in humans. *Clinical Neurophysiology: Official Journal of the International*

Federation of Clinical Neurophysiology, *125*(3), 577–584. https://doi.org/10.1016/j.clinph.2013.09.039

Paxinos, G., & Franklin, K. B. J. (2013). *The Mouse Brain in Stereotaxic Coordinates* (4th ed). Academic Press, San Diego.

Person, A. L., & Raman, I. M. (2011). Purkinje neuron synchrony elicits time-locked spiking in the cerebellar nuclei. *Nature*, *481(7382),* 502–505. https://doi.org/10.1038/nature10732

Pope, P. A., & Miall, R. C. (2012). Task-specific facilitation of cognition by cathodal transcranial direct current stimulation of the cerebellum. *Brain Stimulation*, *5*(2), 84–94. https://doi.org/10.1016/j.brs.2012.03.006

Proville, R. D., Spolidoro, M., Guyon, N., Dugué, G. P., Selimi, F., Isope, P., Popa, D., & Léna, C. (2014). Cerebellum involvement in cortical sensorimotor circuits for the control of voluntary movements. *Nature Neuroscience*, *17*(9), 1233–1239. https://doi.org/10.1038/nn.3773

Ramnani, N. (2006). The primate cortico-cerebellar system: Anatomy and function. *Nature Reviews. Neuroscience*, *7*(7), 511–522. https://doi.org/10.1038/nrn1953

Rezaee, Z., & Dutta, A. (2019). Cerebellar Lobules Optimal Stimulation (CLOS): A Computational Pipeline to Optimize Cerebellar Lobule-Specific Electric Field Distribution. *Frontiers in Neuroscience*, *13*, 266. https://doi.org/10.3389/fnins.2019.00266

Roggeri, L., Rivieccio, B., Rossi, P., & D'Angelo, E. (2008). Tactile stimulation evokes long-term synaptic plasticity in the granular layer of cerebellum. *The Journal of Neuroscience: The Official Journal of the Society for Neuroscience*, *28*(25), 6354–6359. https://doi.org/10.1523/JNEUROSCI.5709-07.2008

Sánchez-León, C. A., Ammann, C., Medina, J. F., & Márquez-Ruiz, J. (2018). Using animal models to improve the design and application of transcranial electrical stimulation in humans. *Current Behavioral Neuroscience Reports*, *5*(2), 125–135. https://doi.org/10.1007/s40473-018-0149-6

Sánchez-León, C. A., Campos, G. S.-G., Fernández, M., Sánchez-López, Á., Medina, J. F., & Márquez-Ruiz, J. (2023). Somatodendritic orientation determines tDCS-induced neuromodulation of Purkinje cell activity in awake mice. *eLife, 13,* RP100941. https://doi.org/10.7554/eLife.100941

Sánchez-León, C. A., Cordones, I., Ammann, C., Ausín, J. M., Gómez-Climent, M. A., Carretero-Guillén, A., Sánchez-Garrido Campos, G., Gruart, A., Delgado-García, J. M., Cheron, G., Medina, J. F., & Márquez-Ruiz, J. (2021). Immediate and after effects of transcranial direct-current stimulation in the mouse primary somatosensory cortex. *Scientific Reports*, *11*(1), 3123. https://doi.org/10.1038/s41598-021-82364-4

Sasaki, K., Kawaguchi, S., Shimono, T., & Yoneda, Y. (1969). Responses evoked in the cerebellar cortex by pontine stimulation. *The Japanese Journal of Physiology*, *19*(1), 95–109. https://doi.org/10.2170/jjphysiol.19.95

Schmahmann, J. D. (2001). The cerebrocerebellar system: Anatomic substrates of the cerebellar contribution to cognition and emotion. *International Review of Psychiatry*, *13*, 247–260. https://doi.org/10.1080/09540260120082092

Schmahmann, J. D., & Sherman, J. C. (1998). The cerebellar cognitive affective syndrome. *Brain: A Journal of Neurology*, *121 (Pt 4)*, 561–579. https://doi.org/10.1093/brain/121.4.561

Shimuta, M., Sugihara, I., & Ishikawa, T. (2020). Multiple signals evoked by unisensory stimulation converge onto cerebellar granule and Purkinje cells in mice. *Communications Biology*, *3*(1), 381. https://doi.org/10.1038/s42003-020-1110-2

Shinoda, Y., Sugiuchi, Y., & Futami, T. (1987). Excitatory inputs to cerebellar dentate nucleus neurons from the cerebral cortex in the cat. *Experimental Brain Research*, *67*(2), 299–315. https://doi.org/10.1007/BF00248551

Siegle, J. H., Pritchett, D. L., & Moore, C. I. (2014). Gamma-range synchronization of fast-spiking interneurons can enhance detection of tactile stimuli. *Nature Neuroscience*, *17*(10), 1371–1379. https://doi.org/10.1038/nn.3797

Spampinato, D., & Celnik, P. (2017). Temporal dynamics of cerebellar and motor cortex physiological processes during motor skill learning. *Scientific Reports*, *7*, 40715. https://doi.org/10.1038/srep40715

Stagg, C. J., Antal, A., & Nitsche, M. A. (2018). Physiology of Transcranial Direct Current Stimulation. *The Journal of ECT*, *34*(3), 144–152. https://doi.org/10.1097/YCT.0000000000000510

Stoodley, C. J., D'Mello, A. M., Ellegood, J., Jakkamsetti, V., Liu, P., Nebel, M. B., Gibson, J. M., Kelly, E., Meng, F., Cano, C. A., Pascual, J. M., Mostofsky, S. H., Lerch, J. P., & Tsai, P. T. (2017). Altered cerebellar connectivity in autism and cerebellar-mediated

rescue of autism-related behaviors in mice. *Nature Neuroscience*, *20*(12), 1744–1751. https://doi.org/10.1038/s41593-017-0004-1

Sugawara, K., Onishi, H., Yamashiro, K., Kojima, S., Miyaguchi, S., Kirimoto, H., Tsubaki, A., Tamaki, H., Shirozu, H., & Kameyama, S. (2015). The effect of anodal transcranial direct current stimulation over the primary motor or somatosensory cortices on somatosensory evoked magnetic fields. *Clinical Neurophysiology: Official Journal of the International Federation of Clinical Neurophysiology*, *126*(1), 60–67. https://doi.org/10.1016/j.clinph.2014.04.014

Sugihara, I. (2011). Compartmentalization of the deep cerebellar nuclei based on afferent projections and aldolase C expression. *Cerebellum (London, England)*, *10*(3), 449–463. https://doi.org/10.1007/s12311-010-0226-1

Sun, Y., Dhamne, S. C., Carretero-Guillén, A., Salvador, R., Goldenberg, M. C., Godlewski, B. R., Pascual-Leone, A., Madsen, J. R., Stone, S. S. D., Ruffini, G., Márquez-Ruiz, J., & Rotenberg, A. (2020). Drug-Responsive Inhomogeneous Cortical Modulation by Direct Current Stimulation. *Annals of Neurology*, *88*(3), 489–502. https://doi.org/10.1002/ana.25822

Swenson, R. S., Sievert, C. F., Terreberry, R. R., Neafsey, E. J., & Castro, A. J. (1989). Organization of cerebral cortico-olivary projections in the rat. *Neuroscience Research*, *7*(1), 43–54. https://doi.org/10.1016/0168-0102(89)90036-9

Tallon-Baudry, C., & Bertrand, O. (1999). Oscillatory gamma activity in humans and its role in object representation. *Trends in Cognitive Sciences*, *3*(4), 151–162. https://doi.org/10.1016/S1364-6613(99)01299-1

Traub, R., & Whittington, M. (2010). *Cortical Oscillations in Health and Disease*. Oxford University Press.

Ugawa, Y., Day, B. L., Rothwell, J. C., Thompson, P. D., Merton, P. A., & Marsden, C. D. (1991). Modulation of motor cortical excitability by electrical stimulation over the cerebellum in man. *The Journal of Physiology*, *441*, 57–72. https://doi.org/10.1113/jphysiol.1991.sp018738

Uhlhaas, P. J., & Singer, W. (2015). Oscillations and neuronal dynamics in schizophrenia: The search for basic symptoms and translational opportunities. *Biological Psychiatry*, *77*(12), 1001–1009. https://doi.org/10.1016/j.biopsych.2014.11.019

Vaseghi, B., Zoghi, M., & Jaberzadeh, S. (2015). Differential effects of cathodal transcranial direct current stimulation of prefrontal, motor and somatosensory cortices on cortical excitability and pain perception—A double-blind randomised sham-controlled study. *The European Journal of Neuroscience*, *42*(7), 2426–2437. https://doi.org/10.1111/ejn.13043

Watson, T. C., Jones, M. W., & Apps, R. (2009). Electrophysiological mapping of novel prefrontal—Cerebellar pathways. *Frontiers in Integrative Neuroscience*, *3*, 18. https://doi.org/10.3389/neuro.07.018.2009

Woods, A. J., Antal, A., Bikson, M., Boggio, P. S., Brunoni, A. R., Celnik, P., Cohen, L. G., Fregni, F., Herrmann, C. S., Kappenman, E. S., Knotkova, H., Liebetanz, D., Miniussi, C., Miranda, P. C., Paulus, W., Priori, A., Reato, D., Stagg, C., Wenderoth, N., & Nitsche, M. A. (2016). A technical guide to tDCS, and related non-invasive brain stimulation tools. *Clinical Neurophysiology: Official Journal of the International Federation of Clinical Neurophysiology*, *127*(2), 1031–1048. https://doi.org/10.1016/j.clinph.2015.11.012

Yosephi, M. H., Ehsani, F., Zoghi, M., & Jaberzadeh, S. (2018). Multi-session anodal tDCS enhances the effects of postural training on balance and postural stability in older adults with high fall risk: Primary motor cortex versus cerebellar stimulation. *Brain Stimulation*, *11*(6), 1239–1250. https://doi.org/10.1016/j.brs.2018.07.044

Zhao, X., Ding, J., Pan, H., Zhang, S., Pan, D., Yu, H., Ye, Z., & Hua, T. (2020). Anodal and cathodal tDCS modulate neural activity and selectively affect GABA and glutamate syntheses in the visual cortex of cats. *The Journal of Physiology*, *598*(17), 3727–3745. https://doi.org/10.1113/JP279340

Zuchowski, M. L., Timmann, D., & Gerwig, M. (2014). Acquisition of conditioned eyeblink responses is modulated by cerebellar tDCS. *Brain Stimulation*, *7*(4), 525–531. https://doi.org/10.1016/j.brs.2014.03.010